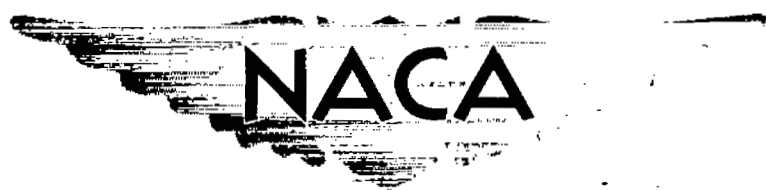


~~CONFIDENTIAL~~

Copy
RM E54F02

NACA RM E54F02



RESEARCH MEMORANDUM

EXPERIMENTAL DATA FOR FOUR FULL-SCALE CONICAL
COOLING-AIR EJECTORS

By C. C. Ciepluch and D. B. Fenn

Lewis Flight Propulsion Laboratory
Cleveland, Ohio

CLASSIFICATION CHANGED

To UNCLASSIFIED

By authority of NACA Res also effective
+ RN-128 Date June 24, 1958
Am 8-12-58

CLASSIFIED DOCUMENT

This material contains information affecting the National Defense of the United States within the meaning of the espionage laws, Title 18, U.S.C., Secs. 793 and 794, the transmission or revelation of which in any manner to an unauthorized person is prohibited by law.

NATIONAL ADVISORY COMMITTEE
FOR AERONAUTICS

WASHINGTON

November 1, 1954

~~CONFIDENTIAL~~



NATIONAL ADVISORY COMMITTEE FOR AERONAUTICS

RESEARCH MEMORANDUM

EXPERIMENTAL DATA FOR FOUR FULL-SCALE CONICAL COOLING-AIR EJECTORS

By C. C. Ciepluch and D. B. Fenn

SUMMARY

An experimental investigation was conducted to determine the pumping and thrust characteristics of four full-scale conical air ejectors over a range of primary gas temperature. The fixed ejector configurations simulated a variable-primary-nozzle-area and variable-diameter-ratio ejector which operated at diameter ratios of 1.11 and 1.31 for nonafterburning and afterburning flight conditions, respectively. Performance data were obtained at spacing ratios of 0.4 and 0.8.

The spacing ratio influenced both ejector pumping and thrust performance. The pumping characteristics of the configurations with spacing ratios of 0.8 were generally better at the lower weight-flow ratios. However, the ejector jet-thrust ratio of the configurations with the spacing ratio of 0.4, in general, exceeded that of the configurations with spacing ratios of 0.8 for the lower values of weight-flow ratio.

INTRODUCTION

The air ejector is considered an effective means of providing cooling air for aircraft engine installations. Ejector performance, however, is influenced by both geometrical and operational variables. Although a large amount of model ejector test data exists, only a limited quantity of full-scale data is available. References 1 to 6 present ejector performance data on both conical and cylindrical models over a wide range of geometrical and operational variables at primary- to secondary-temperature ratios of 1.0. Performance data on various full-scale ejector configurations at several primary gas temperatures are available in references 7 and 8.

In order to provide additional information on full-scale cooling-air ejector performance, a general program for the experimental investigation of full-scale ejectors has been conducted at the NACA Lewis laboratory. As part of this program, an investigation was conducted to determine the pumping and thrust characteristics of four conical cooling-air ejectors having large primary-nozzle conical half-angles. The experimental results of this investigation are reported herein.

3399

OK-1

The fixed ejector configurations investigated simulated a variable-primary-nozzle-area and variable-diameter-ratio ejector which operated at diameter ratios of 1.11 and 1.31 for nonafterburning and afterburning flight conditions, respectively. Performance data were obtained for the simulated ejector configuration at spacing ratios of 0.4 and 0.8.

Air pumping and thrust performance data were obtained over a range of primary-nozzle pressure ratio from 1.5 to 7.0. The nonafterburning configurations were run with primary gas temperatures from 1220° to 1500° R, while the afterburning configurations were run at primary gas temperatures of approximately 1140°, 2000°, and 3300° R.

APPARATUS

Test Facility

A turbojet engine equipped with an afterburner was used as the gas generator for the ejector investigation. The installation of the engine and afterburner in an altitude test chamber is shown in figures 1 and 2, and a sketch of the afterburner shell and exhaust nozzles is shown in figure 3. The engine and afterburner assembly was rigidly mounted on a platform which was suspended by means of flexure plates. Forces acting on the engine were transmitted from the platform to a calibrated thrust-measuring unit.

Ejector Configurations

The four ejector configurations investigated are listed in the following table with a summary of the range of conditions covered:

Configuration	Diameter ratio, D_s/D_p	Spacing ratio, L/D_p	Primary gas temperature, °R	Measured weight-flow ratio, W_s/W_p
1	1.11	0.39	1220 1500	0 to 0.155 0 to .145
2	1.11	0.78	1220 1500	0 to 0.155 0 to .150
3	1.31	0.4	1140 2050 3250 to 3400	0 to 0.243 .039 to .20 .059 to .231
4	1.31	0.81	1140 1900 to 2000 3200 to 3400	0 to 0.200 0 to .16 .064 to .240

The dimensions of both the primary nozzles and the secondary shrouds are given for each configuration in figure 4. A list of the symbols used throughout this report is included in appendix A.

INSTRUMENTATION

Primary Stream

The primary-nozzle total pressure was measured by a 12-probe, diametrical, water-cooled rake (station P, fig. 4) located 5 inches upstream of the end of the cylindrical afterburner shell. Each probe was located on a center of equal annular flow areas. Four equally spaced wall static taps were also located at station P. The primary gas temperature was measured for nonafterburning operation by 48 thermocouples at the turbine outlet. For afterburner operation the primary gas temperature was calculated as described in appendix B. Primary-nozzle skin temperatures were measured in order to determine the thermal expansion.

Secondary Stream

The secondary total pressure was measured 2 inches upstream of the end of the afterburner shell (station S) by eight total-pressure probes located circumferentially around the annular secondary passage. Four temperature probes measured the total temperature of the secondary stream at station S.

The ejector ambient pressure was measured by four equally spaced static-pressure tubes located on the outside lip of the ejector shroud. The effective primary-nozzle exhaust pressure was also measured by lip static-pressure tubes. Wall static-pressure taps were provided to measure the wall pressure distribution on each ejector shroud.

Air-Flow Measurement

Engine air flow was calculated from total- and static-pressure and total-temperature measurements obtained in a venturi upstream of the engine inlet. Secondary air flow was calculated from an instrumented A.S.M.E. flat-plate orifice.

PROCEDURE

Ejector performance data were obtained over a range of ejector weight-flow ratio W_s/W_p and primary gas temperature. At each given ejector weight-flow ratio and primary gas temperature, the primary-nozzle pressure ratio P_p/p_0 was varied from about 1.5 to 7.0.

Primary-nozzle calibrations were obtained with ejector shrouds removed at primary gas temperatures from 1140° to 1500° R.

Clear unleaded gasoline (MIL-F-5572, 115/145) was used as the engine fuel, and MIL-F-5624A grade JP-4 was used for afterburner fuel throughout the investigation.

DATA PRESENTATION

Ejector Performance

Pumping characteristics. - The pumping characteristics are presented as plots of secondary pressure ratio P_s/p_0 against primary-nozzle pressure ratio P_p/p_0 at constant values of ejector weight-flow ratio W_s/W_p for each primary-nozzle gas temperature. Figure 5 shows the pumping characteristics of configurations 1 to 4. The nominal temperature ratio T_p/T_s (ratio of primary gas total temperature to secondary gas total temperature), which was nearly constant for each ejector weight-flow ratio, is also included.

Thrust performance. - The influence of primary-nozzle pressure ratio on ejector jet-thrust ratio for constant values of ejector weight-flow ratio is shown in figure 6 at various primary gas temperatures for configurations 1 to 4. Ejector jet-thrust ratio is defined as the ratio of the ejector (gross) jet thrust to the jet thrust of the primary conical nozzle operating at the same over-all primary pressure ratio P_p/p_0 .

Ejector performance is influenced by size and shape of the secondary flow passage as well as by ejector geometry. Therefore, only configurations having secondary flow passages and ejector geometry similar to those reported herein can be expected to have the same pumping and thrust characteristics.

Effect of Ejector Spacing Ratio on Ejector Performance

Pumping characteristics. - The effect of spacing ratio (ratio of the axial distance between the primary nozzle and the ejector exit to the diameter of the primary nozzle) on the air pumping characteristics of configurations 1 and 2, which had a diameter ratio of 1.11 and spacing ratios of 0.4 and 0.8, respectively, is shown in figure 7(a) at a primary gas temperature of 1220° R. For primary-nozzle pressure ratios less than 3.0, configuration 2 (spacing ratio of 0.8) is superior in air pumping capacity to configuration 1 (spacing ratio of 0.4) for weight-flow ratios of approximately 3 percent. Because the ejector-shroud exit was relatively farther away from the primary-nozzle

exit as the spacing ratio increased, a lower primary-nozzle pressure ratio was required to expand the primary jet until it filled the secondary shroud and thus reached its maximum air pumping capacity. At primary-nozzle pressure ratios above 3.0 and an air-flow ratio of 0.03, the air pumping ability of configuration 1 (spacing ratio of 0.4) exceeded that of configuration 2 (spacing ratio of 0.8). At higher weight-flow ratios (about 10 percent), the effect of spacing ratio on pumping capacity was small over the entire range of primary pressure ratio.

The influence of spacing ratio on the pumping characteristics of configurations 3 and 4, which had diameter ratios of 1.31 and spacing ratios of 0.4 and 0.8, respectively, is shown in figure 7(b) at a primary gas temperature of approximately 3300° R. The air pumping advantage of configuration 4 (spacing ratio of 0.8) over configuration 3 (spacing ratio of 0.4) occurs over the entire range of primary-nozzle pressure ratio at an air-flow ratio of 0.08. The differences between the results of figures 8(a) and (b) are due to the differences in diameter ratio.

Thrust performance. - The influence of spacing ratio on the ejector jet-thrust ratio is shown in figure 8(a) for the configurations with diameter ratios of 1.11 (1 and 2) at a primary gas temperature of 1220° R and in figure 8(b) for the configurations with diameter ratios of 1.31 (3 and 4) at a primary gas temperature of approximately 3300° R. Configuration 1 (spacing ratio of 0.4, fig. 8(a)) had an ejector jet-thrust ratio 2 to 5 percent greater than that of configuration 2 (spacing ratio of 0.8) over the range of weight-flow ratio investigated.

The jet-thrust ratio of configuration 3 (spacing ratio of 0.4) exceeded that of configuration 4 (spacing ratio of 0.8) by up to 2 percent at a weight-flow ratio of about 0.08 at primary-nozzle pressure ratios less than 4 (fig. 8(b)). For higher nozzle pressure ratios this trend was reversed. The thrust ratio of configuration 4 exceeded that of configuration 3 by 3 percent at a nozzle pressure ratio of 6 for a weight-flow ratio of 0.20.

Ejector-Shroud Wall Pressure Distribution

Ejector-shroud wall pressure distributions of configurations 1 to 4 are shown in figure 9(a) to (d) at zero weight-flow ratio for several primary-nozzle pressure ratios.

In figure 9(e) the ejector-shroud wall pressure distributions (ratio of shroud wall pressure to secondary total pressure) of configuration 3 are shown for several primary-nozzle pressure ratios at a weight-flow ratio of 0.191. Minimum secondary-passage flow area existed between the cylindrical afterburner shell and the ejector cooling shroud. The secondary passage area increased rapidly downstream of the minimum area until

it was several times larger at the primary-nozzle exit, as shown in the sketch in figure 9(e). The secondary passage therefore consisted of a convergent-divergent flow channel. At the higher secondary weight-flow ratios, supersonic flow was encountered in the secondary passage resulting from overexpansion (fig. 9(e)). The overexpansion resulted in shock and diffusion losses in the secondary stream which probably compromised both the pumping and thrust performance of these configurations.

Lewis Flight Propulsion Laboratory
National Advisory Committee for Aeronautics
Cleveland, Ohio, June 16, 1954

3399

APPENDIX A

SYMBOLS

The following symbols are used in this report:

A	area, sq ft
C_D	primary-nozzle flow coefficient, ratio of measured mass flow to isentropic mass flow
C_X	ratio of heated to cold primary-nozzle throat area
D_p	exit diameter of primary nozzle, in.
D_s	exit diameter of ejector shroud, in.
F	jet thrust (gross thrust), lb
F_d	force of thrust measuring unit, lb
g	acceleration due to gravity, 32.17 ft/sec ²
L	axial distance between exit planes of primary nozzle and ejector shroud, in.
P	total pressure, lb/sq ft abs
p	static pressure, lb/sq ft abs
R	gas constant, 53.4 ft-lb/(lb)(°R)
T	total temperature, °R
V	velocity, ft/sec
W	weight flow, lb/sec
γ	ratio of specific heats of gas

Subscripts:

a	engine
at	atmospheric

e effective
ej ejector jet
f fuel
i isentropic
j primary jet
L lip
l labyrinth seal
p primary stream or nozzle
r thrust rod
s secondary stream
w wall
0 ambient exhaust
1 engine inlet
2 air-flow measurement
3 ejector exit
4 secondary air inlet

APPENDIX B

METHODS OF CALCULATION

Air flow. - Engine air flow W_a was calculated from measurements of total and static pressures and total temperature obtained at station 2 (fig. 1) in the following manner:

$$W_a = \frac{P_2 A_2}{\sqrt{RT_2}} \sqrt{\frac{2g\gamma}{\gamma-1} \left[\left(\frac{P_2}{P_2} \right)^{\frac{\gamma-1}{\gamma}} - 1 \right] \left(\frac{P_2}{P_2} \right)^{\frac{\gamma-1}{\gamma}}}$$

The primary-nozzle weight flow was determined as follows:

$$W_p = W_a + W_f$$

where W_f was equal to the total fuel flow. Secondary air flow was measured with an A.S.M.E. standard flat-plate orifice.

The flow coefficients of the primary nozzles were calculated from tests with the ejector shroud removed as follows:

$$C_D = \frac{\text{measured weight flow}}{\text{isentropic weight flow}} = \frac{W_p}{W_i}$$

The isentropic weight flow was determined from the following relation:

$$W_i = \frac{P_p A_p C_X}{\sqrt{RT_p}} \sqrt{\frac{2g\gamma_p}{\gamma-1} \left[\left(\frac{p}{P_p} \right)^{\frac{2}{\gamma_p}} - \left(\frac{p}{P_p} \right)^{\frac{\gamma_p+1}{\gamma_p}} \right]}$$

The value of γ_p was determined from the fuel-air ratio and the primary gas temperature as described in reference 9. For critical flow, p/P_p equaled $\left(\frac{\gamma_p+1}{2} \right)^{\frac{\gamma_p}{\gamma_p-1}}$; or for subcritical flow, p/P_p equaled p_0/P_p . The term C_X is the ratio of heated to cold primary-nozzle throat area and is based on the primary-nozzle skin temperature and the thermal expansion coefficient.

Primary gas temperature. - For the afterburning conditions the primary gas temperature was calculated from the following relation:

$$T_p = \left[\frac{\left(\frac{p}{p_p}\right) p_p A_p C_D C_X}{W_p} \sqrt{\frac{2g\gamma}{R(\gamma-1)} \left[\left(\frac{p}{p_p}\right)^{\frac{\gamma-1}{\gamma}} - 1 \right] \left(\frac{p}{p_p}\right)^{\frac{\gamma-1}{\gamma}}} \right]$$

This equation was evaluated by trial and error. A value of γ was assumed. The effective primary-nozzle pressure ratio was determined by means of a lip static pressure measured in the plane of the primary-nozzle exit as shown in figure 4. For critical flow, p/p_p equaled $\left(\frac{\gamma+1}{2}\right)^{\frac{\gamma}{\gamma-1}}$; or for subcritical flow, p/p_p equaled p_L/p_p .

Thrust. - The jet thrust of each configuration was calculated in the following manner:

$$F_{ej} = \frac{W_3}{g} V_3 + A_3(p_3 - p_0)$$

$$F_{ej} = A_L(p_L - p_0) + p_4 A_4 + \frac{W_4}{g} V_4 + p_{4,L} A_{4,L} + F_d + A_r(p_{at} - p_0)$$

The ejector jet-thrust ratio was defined as the ratio of the ejector jet thrust to the jet thrust of the primary nozzle operating at the same over-all primary-nozzle pressure ratio

$$\frac{F_{ej}}{F_j} = \frac{\text{ejector jet thrust}}{\text{jet thrust of primary nozzle}}$$

The jet thrust of the primary nozzle was obtained from calibrations of both the 16.21-inch- and 19.58-inch-diameter primary nozzles. The results of these calibrations are shown in figure 10 in which the thrust parameter $F_j/p_0 A_p$ is plotted against primary-nozzle pressure ratio.

The thrust parameters of an ideal convergent nozzle and for isentropic expansion are also included in figure 10. The flow coefficients of both primary nozzles were also obtained during these calibrations and are shown in figure 11(a) and (b) for the 16.21-inch- and 19.58-inch-diameter nozzles, respectively.

REFERENCES

1. Ellis, C. W., Hollister, D. P., and Sargent, A. F., Jr.: Preliminary Investigation of Cooling-Air Ejector Performance at Pressure Ratios from 1 to 10. NACA RM E51H21, 1951.

2. Greathouse, W. K., and Hollister, D. P.: Preliminary Air-Flow and Thrust Calibrations of Several Conical Cooling-Air Ejectors with a Primary to Secondary Temperature Ratio of 1.0. I - Diameter Ratios of 1.2 and 1.10. NACA RM E52E21, 1952.
3. Greathouse, W. K., and Hollister, D. P.: Preliminary Air-Flow and Thrust Calibrations of Several Conical Cooling Air-Ejectors with a Primary to Secondary Temperature Ratio of 1.0. II - Diameter Ratios of 1.06 and 1.40. NACA RM E52F26, 1952.
4. Greathouse, W. K., and Hollister, D. P.: Air-Flow and Thrust Characteristics of Several Cylindrical Cooling-Air Ejectors with a Primary to Secondary Temperature Ratio of 1.0. NACA RM E52L24, 1953.
5. Huntley, S. C., and Yanowitz, Herbert: Pumping and Thrust Characteristics of Several Divergent Cooling-Air Ejectors and Comparison of Performance with Conical and Cylindrical Ejectors. NACA RM E53J13, 1954.
6. Kochendorfer, Fred D., and Rouso, Morris D.: Performance Characteristics of Aircraft Cooling Ejectors Having Short Cylindrical Shrouds. NACA RM E51E01, 1951.
7. Wallner, Lewis E., and Jansen, Emmert T.: Full-Scale Investigation of Cooling Shroud and Ejector Nozzle for a Turbojet Engine - Afterburner Installation. NACA RM E51J04, 1951.
8. Greathouse, W. K.: Preliminary Investigation of Pumping and Thrust Characteristics of Full-Size Cooling-Air Ejectors at Several Exhaust-Gas Temperatures. NACA RM E54A18, 1954.
9. Turner, L. Richard, Addie, Albert N., and Zimmerman, Richard H.: Charts for the Analysis of One-Dimensional Steady Compressible Flow. NACA TN 1419, 1948.

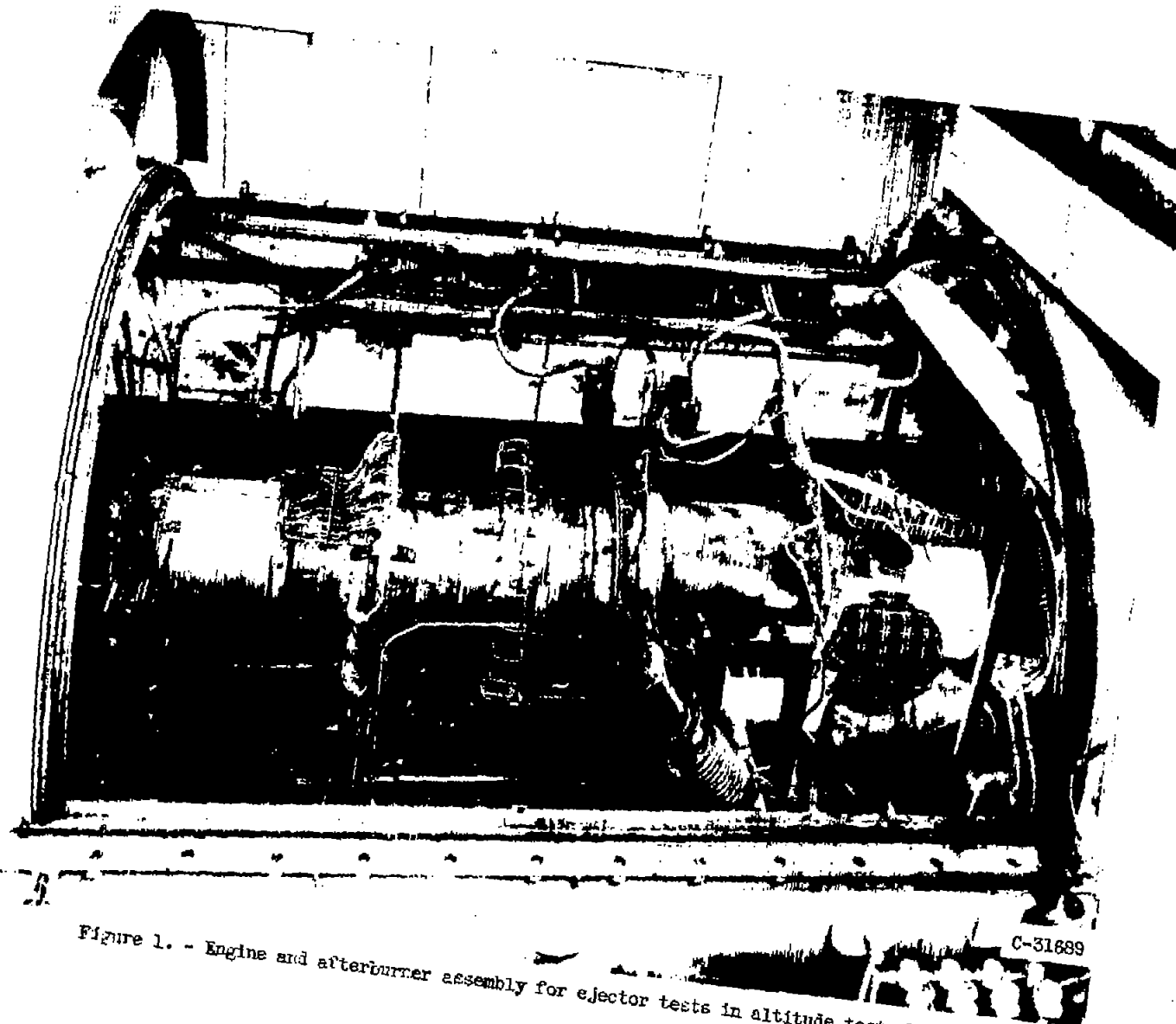


Figure 1. - Engine and afterburner assembly for ejector tests in altitude test chamber.

C-31889

NACA RM B54F02

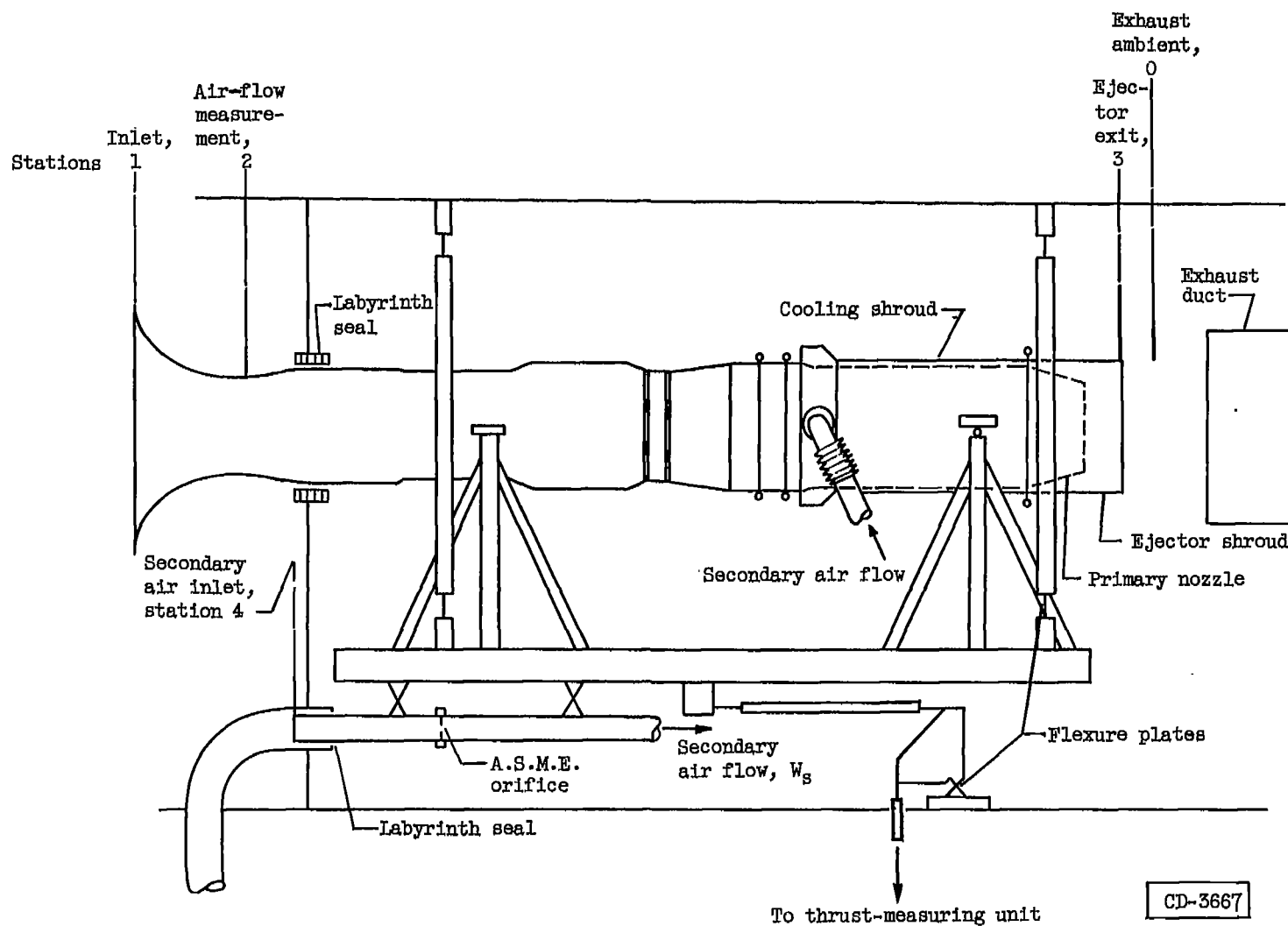


Figure 2. - Diagram of ejector test setup in altitude test chamber.

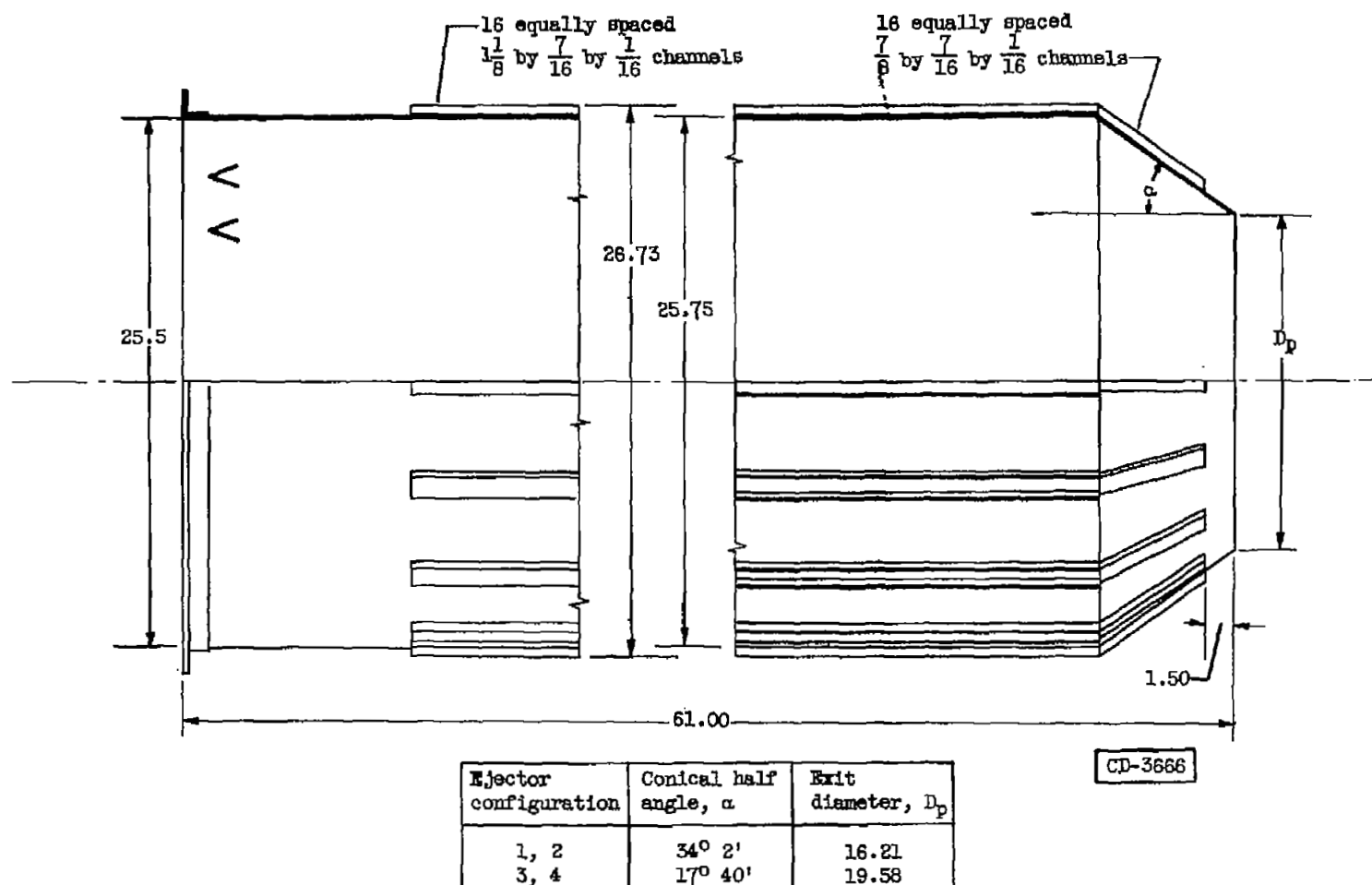
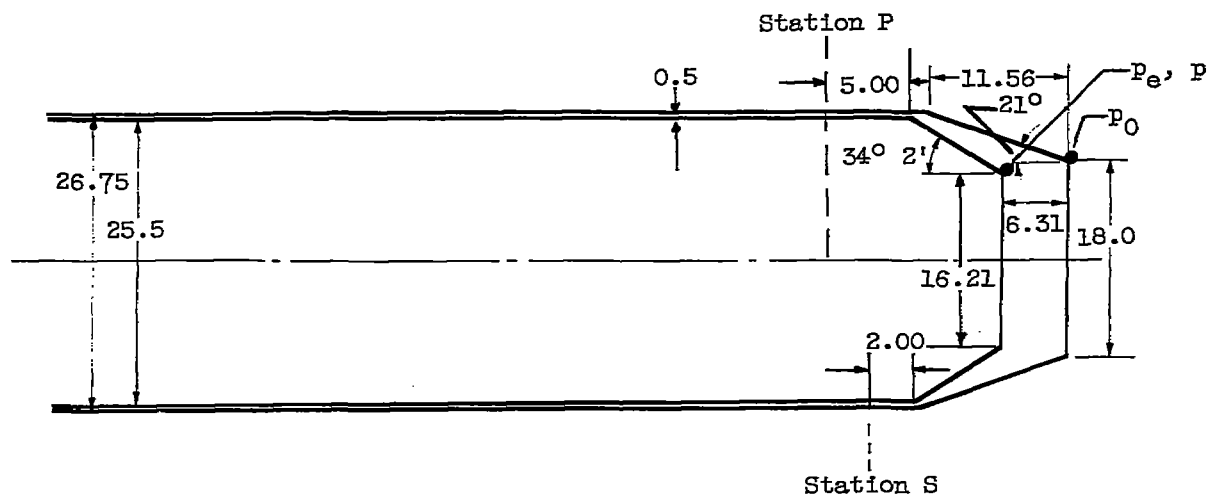
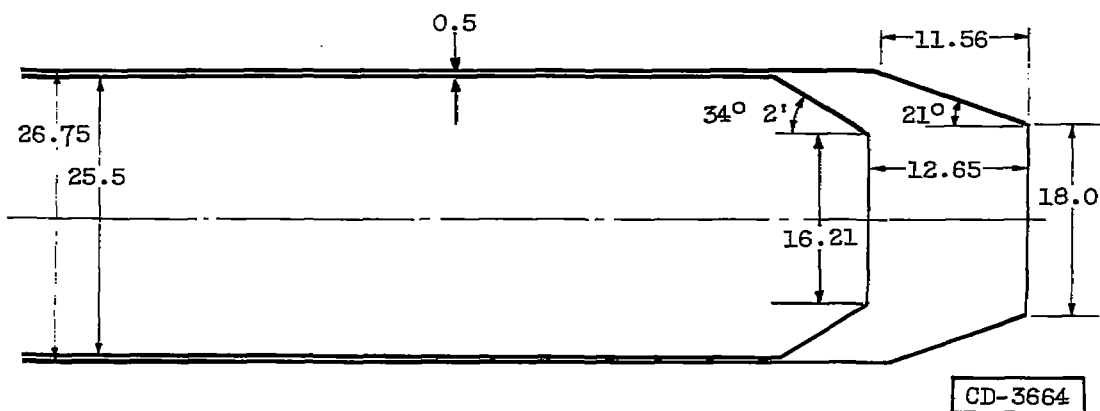


Figure 3. - Afterburner shell (dimensions in inches).

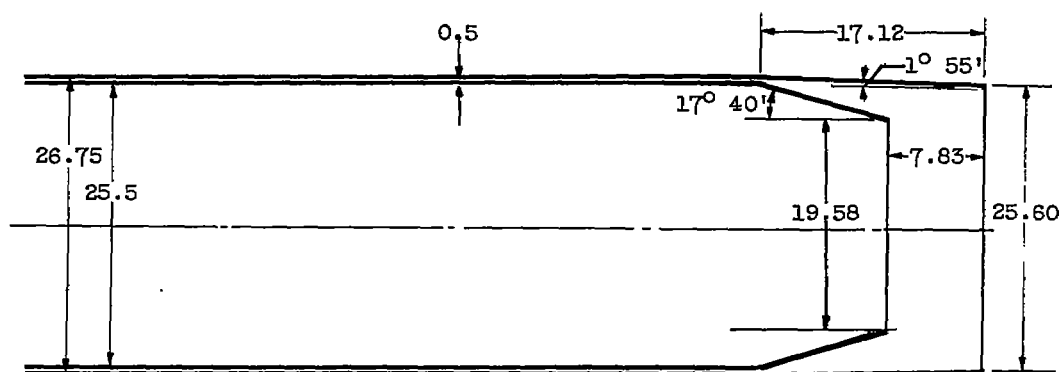


(a) Configuration 1; diameter ratio, 1.11; spacing ratio, 0.39.

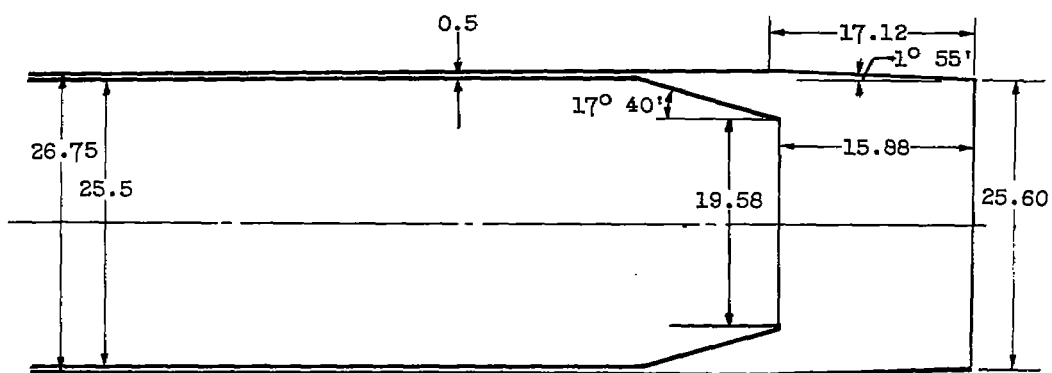


(b) Configuration 2; diameter ratio, 1.11; spacing ratio, 0.78.

Figure 4. - Dimensions of ejector configurations (dimensions in inches).



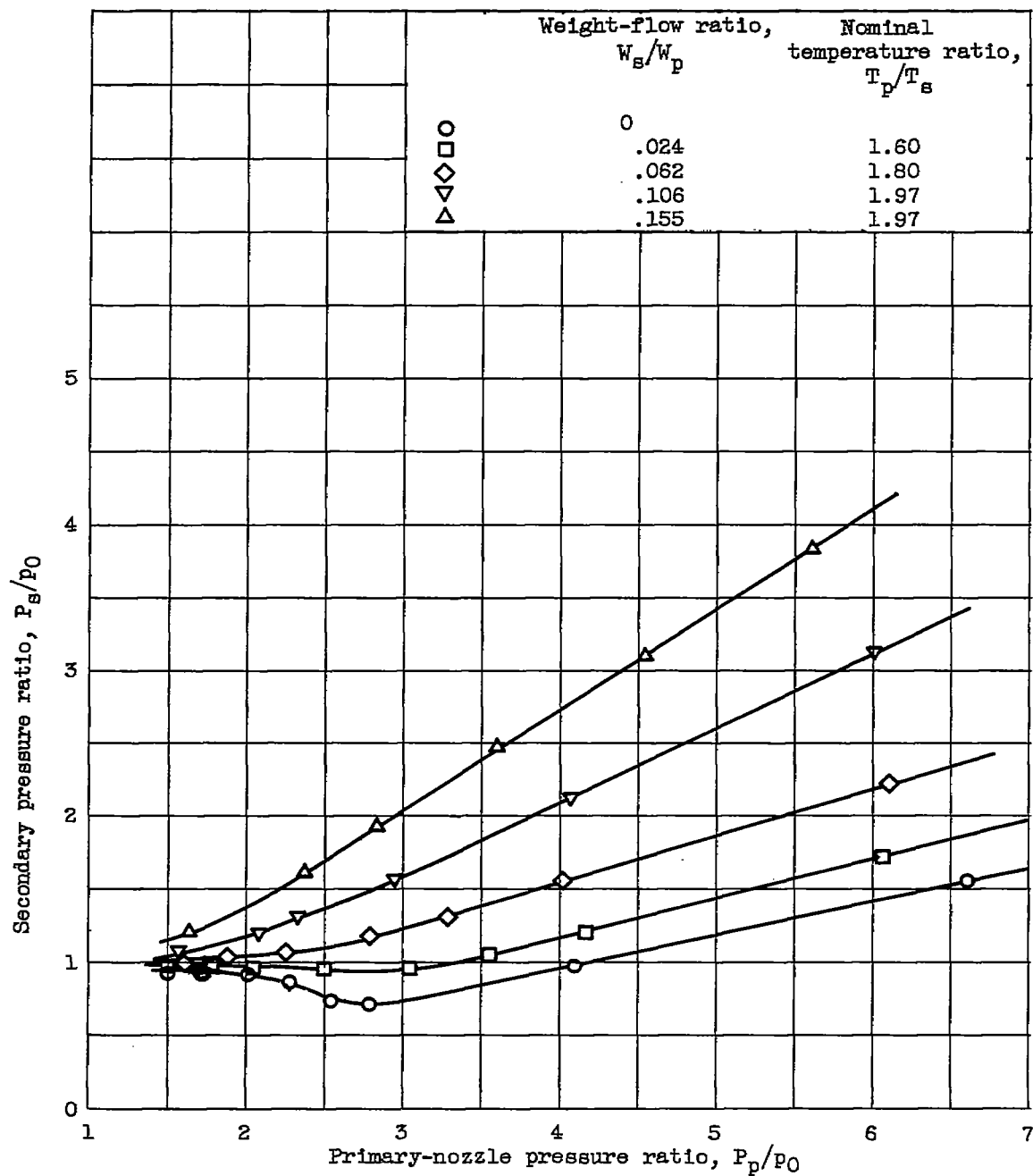
(c) Configuration 3; diameter ratio, 1.31; spacing ratio, 0.4.



CD-3665

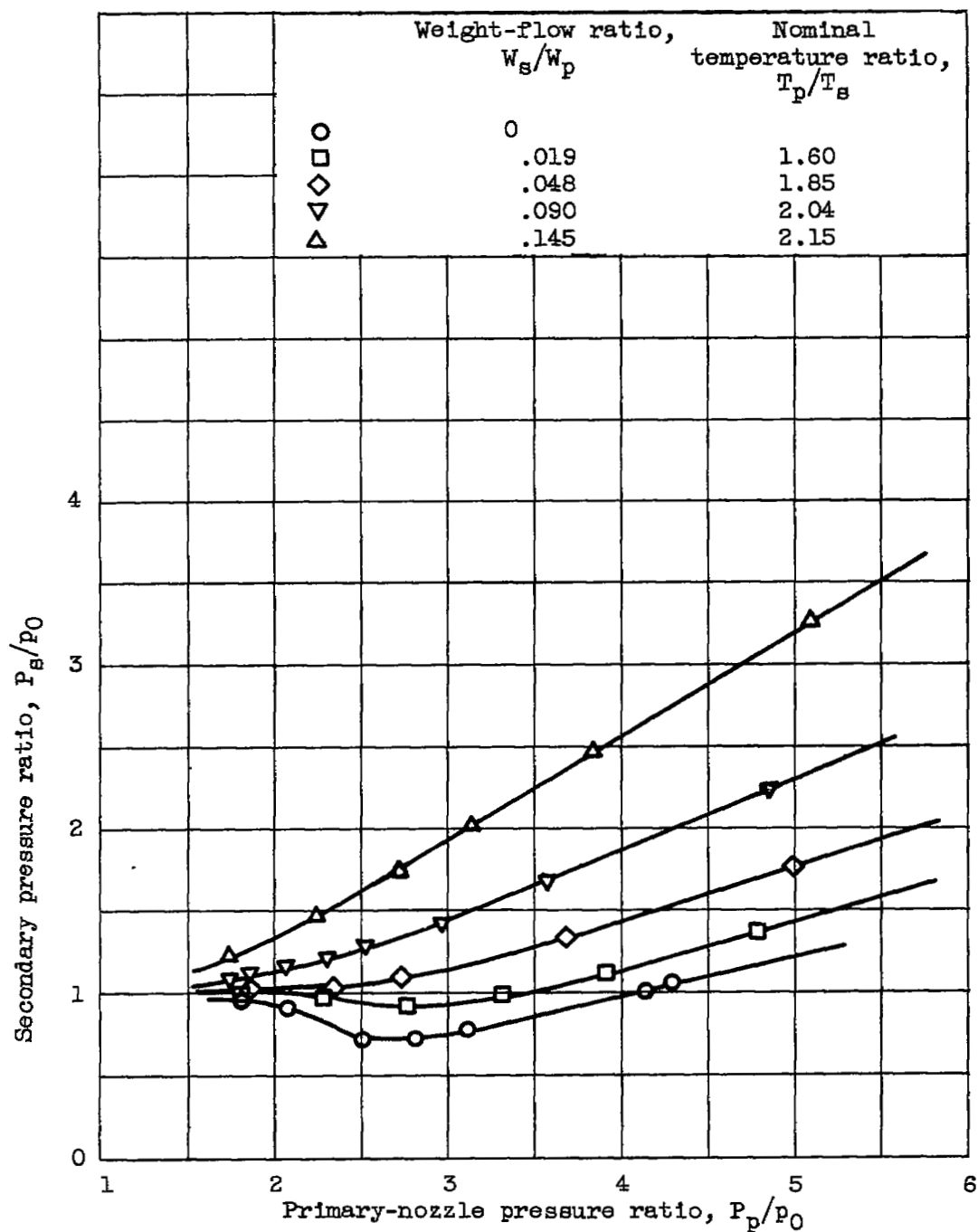
(d) Configuration 4; diameter ratio, 1.31; spacing ratio, 0.81.

Figure 4. - Concluded. Dimensions of ejector configurations (dimensions in inches).



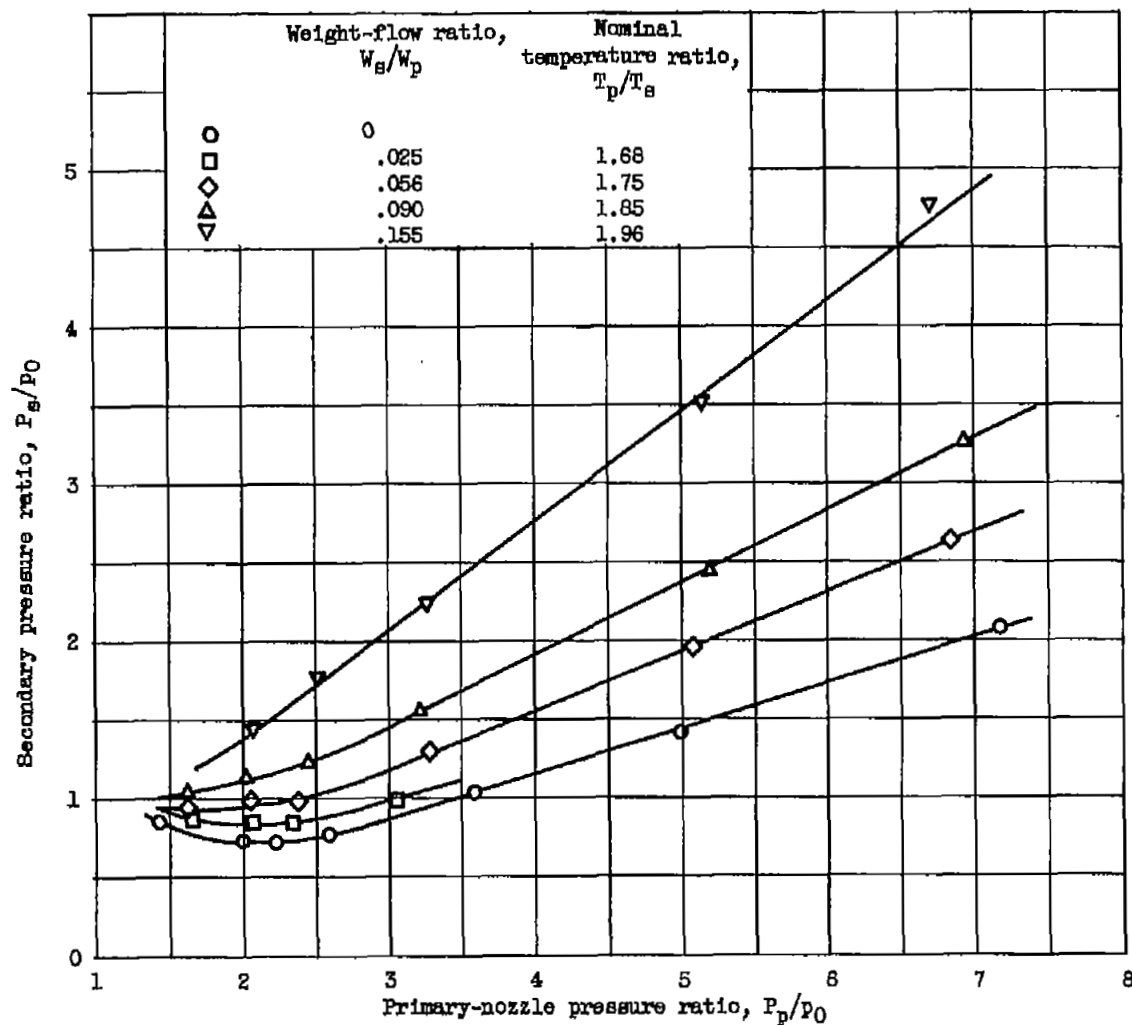
(a) Configuration 1; primary gas temperature, 1220° R; diameter ratio, 1.11; spacing ratio, 0.39.

Figure 5. - Ejector pumping characteristics.



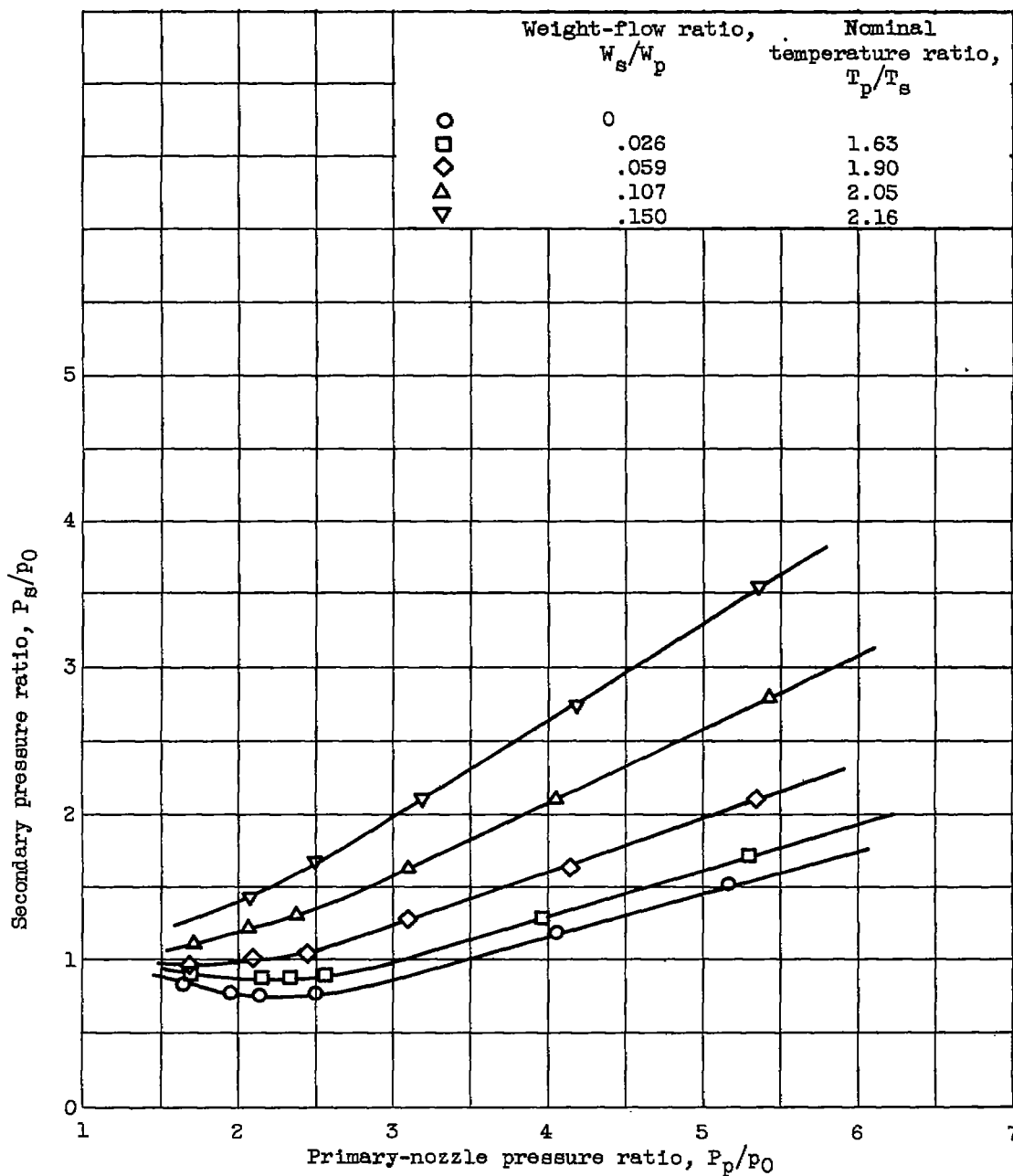
(b) Configuration 1; primary gas temperature, 1500° R; diameter ratio, 1.11; spacing ratio, 0.39.

Figure 5. - Continued. Ejector pumping characteristics.



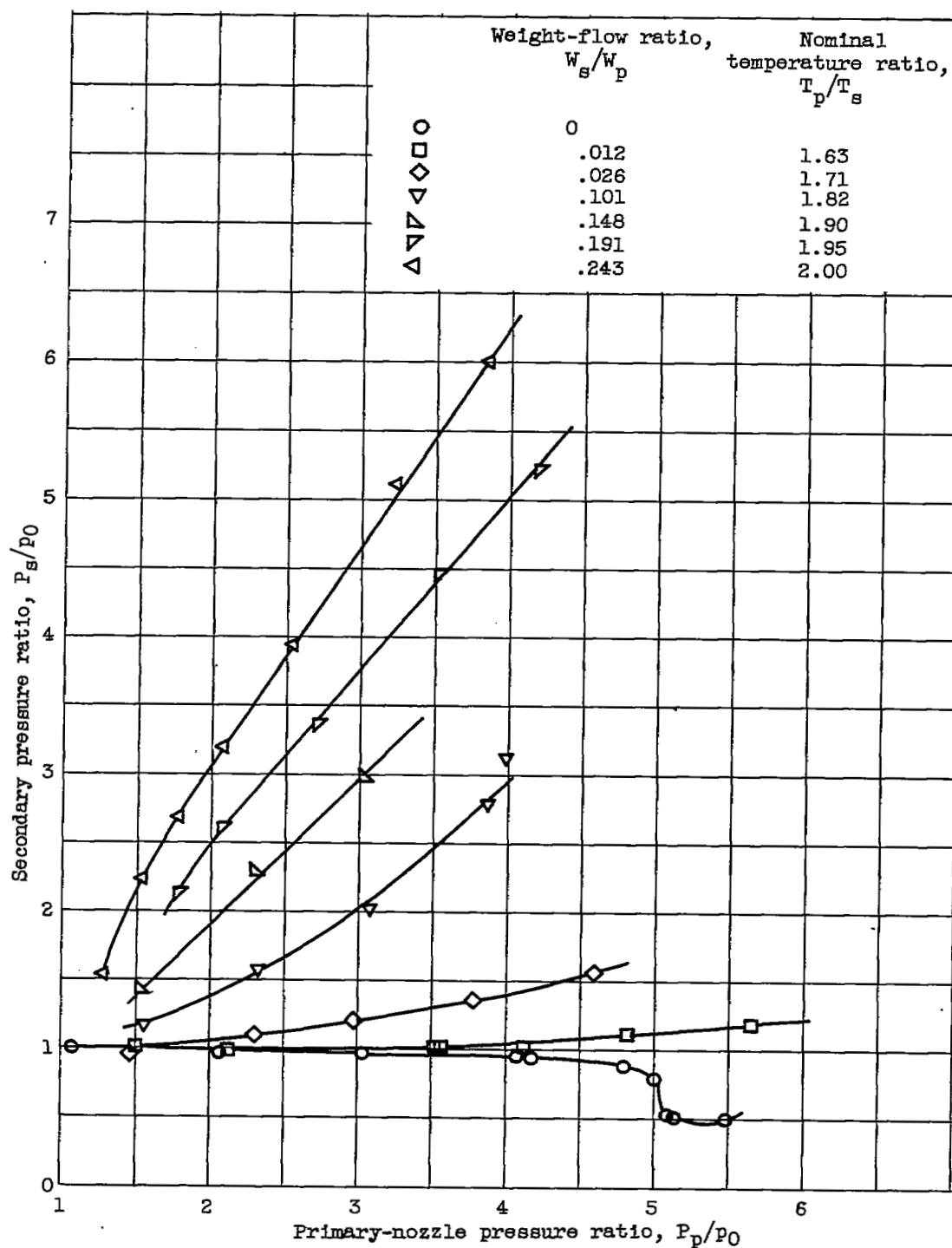
(c) Configuration 2; primary gas temperature, 1220° R; diameter ratio, 1.11; spacing ratio, 0.78.

Figure 5. - Continued. Ejector pumping characteristics.



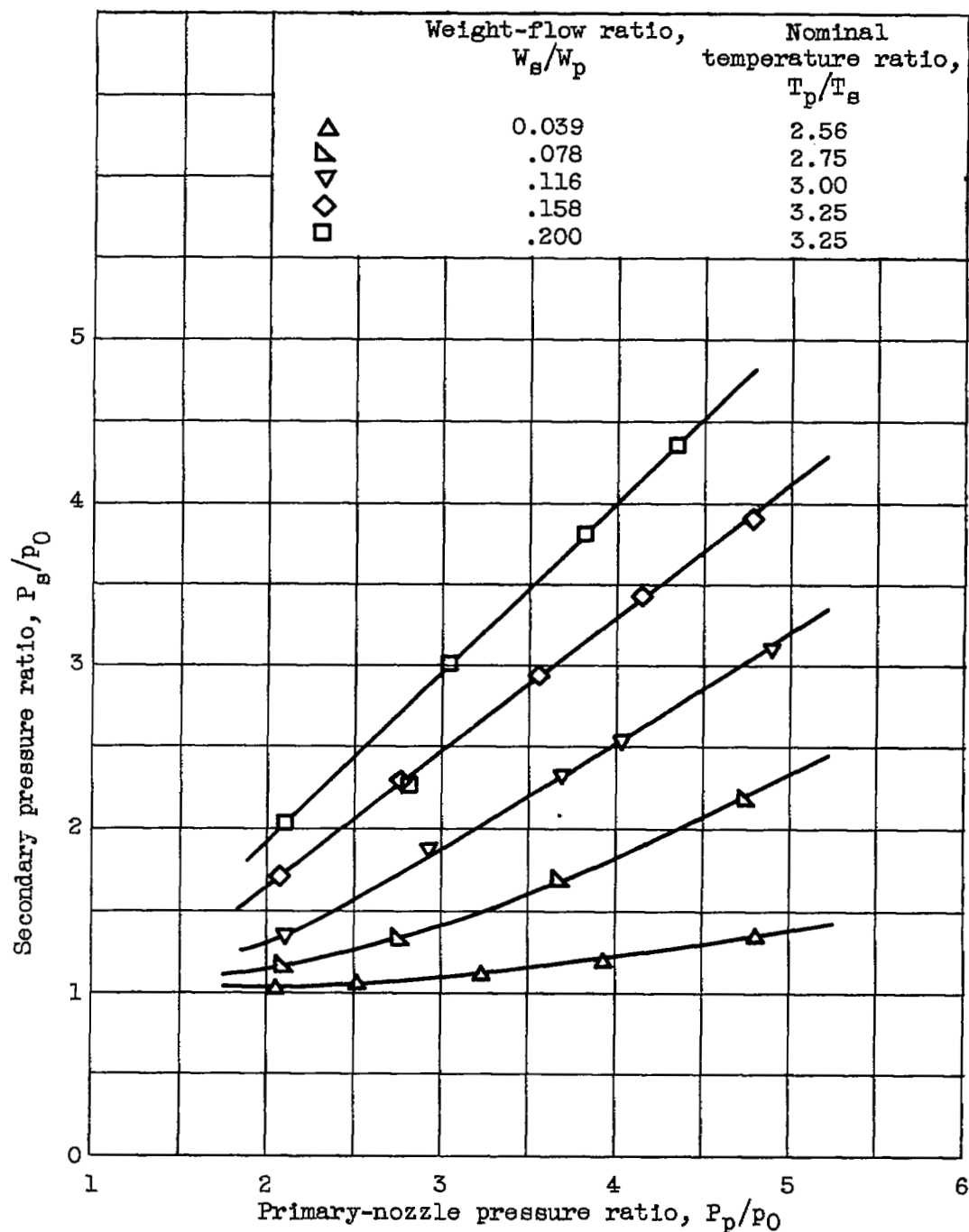
(d) Configuration 2; primary gas temperature, 1500° R; diameter ratio, 1.11; spacing ratio, 0.78.

Figure 5. - Continued. Ejector pumping characteristics.



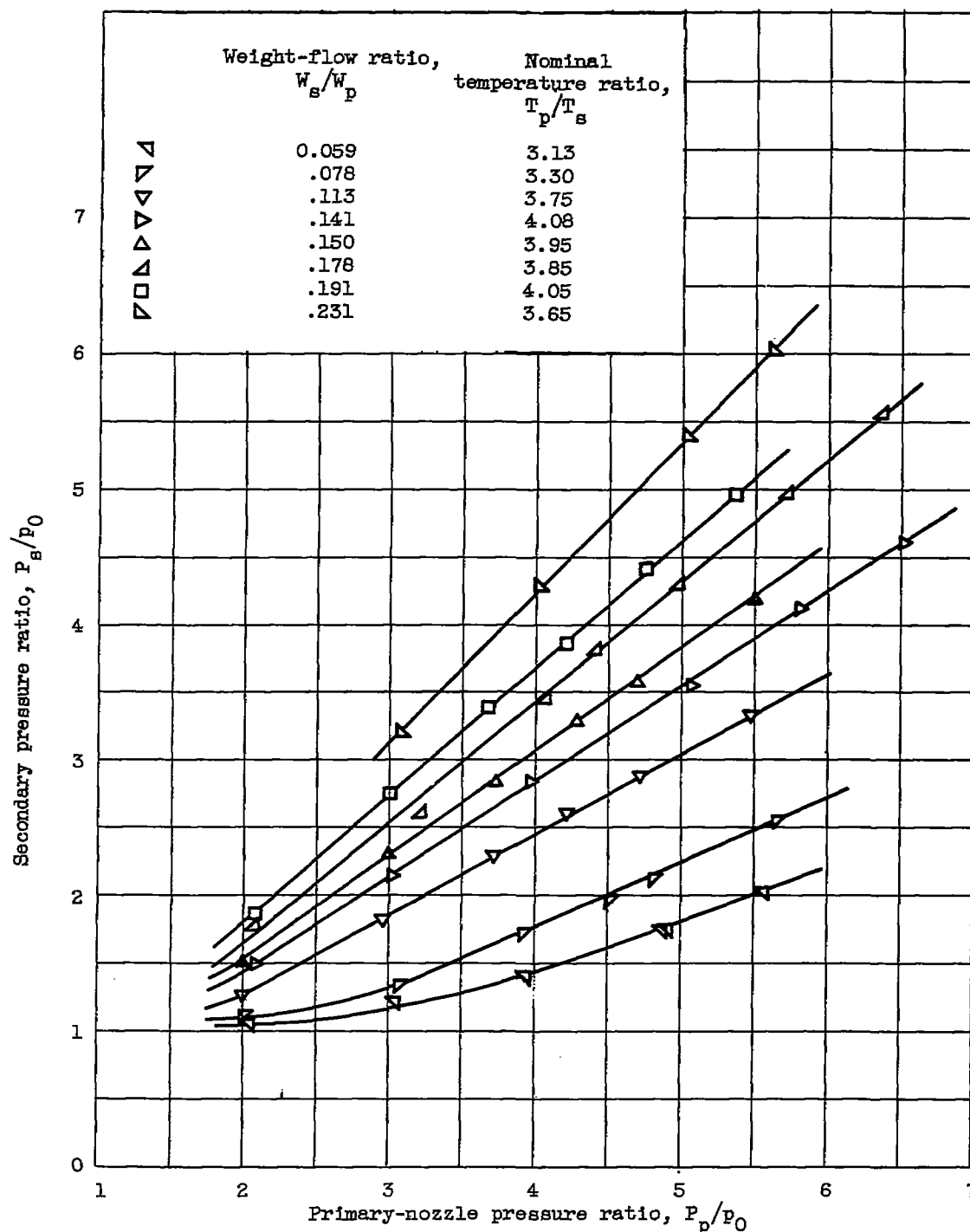
(e) Configuration 3; primary gas temperature, 1140° R; diameter ratio, 1.31; spacing ratio, 0.4.

Figure 5. - Continued. Ejector pumping characteristics.



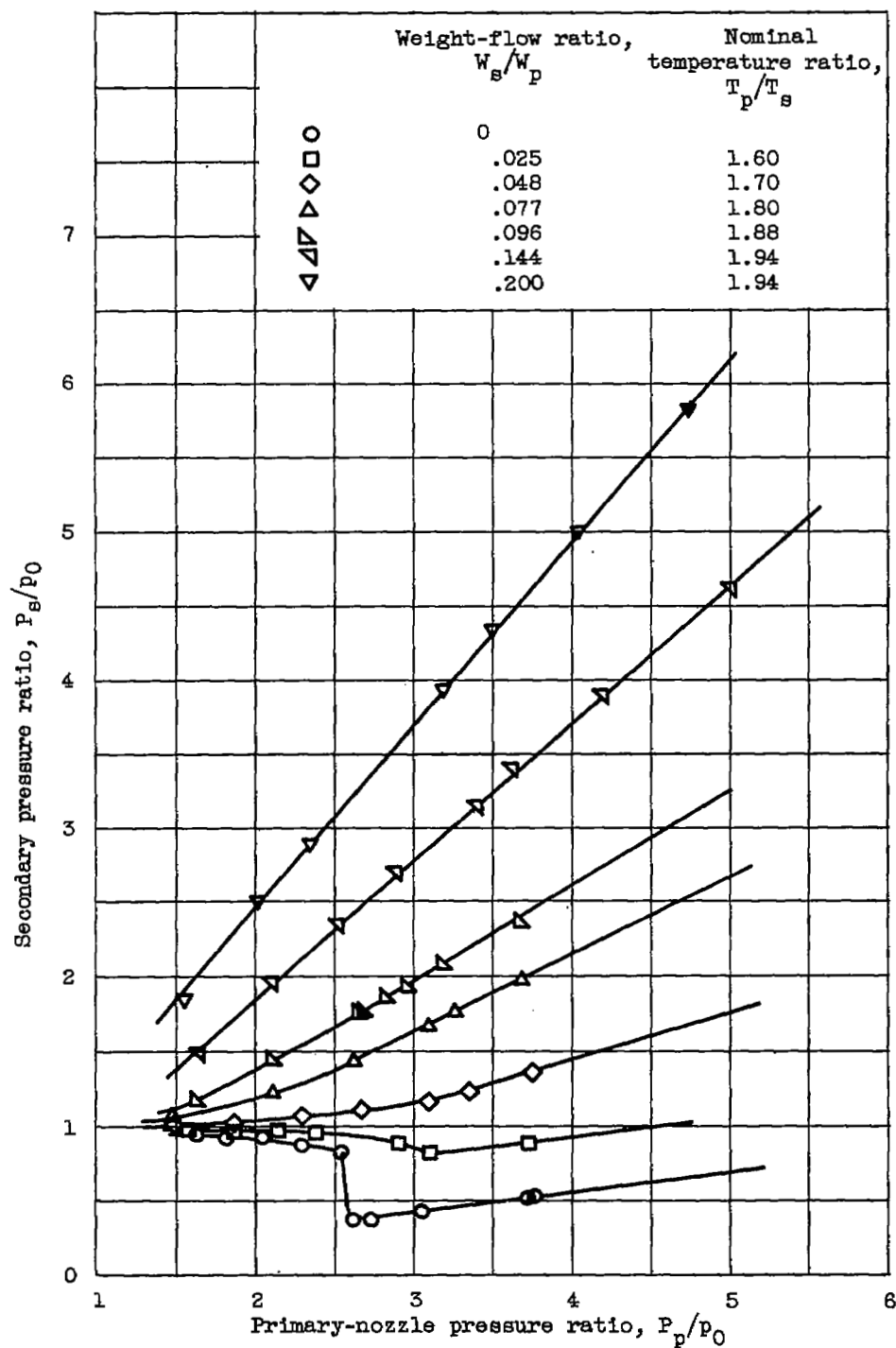
(f) Configuration 3; primary gas temperature, 2050° R; diameter ratio, 1.31; spacing ratio, 0.4.

Figure 5. - Continued. Ejector pumping characteristics.



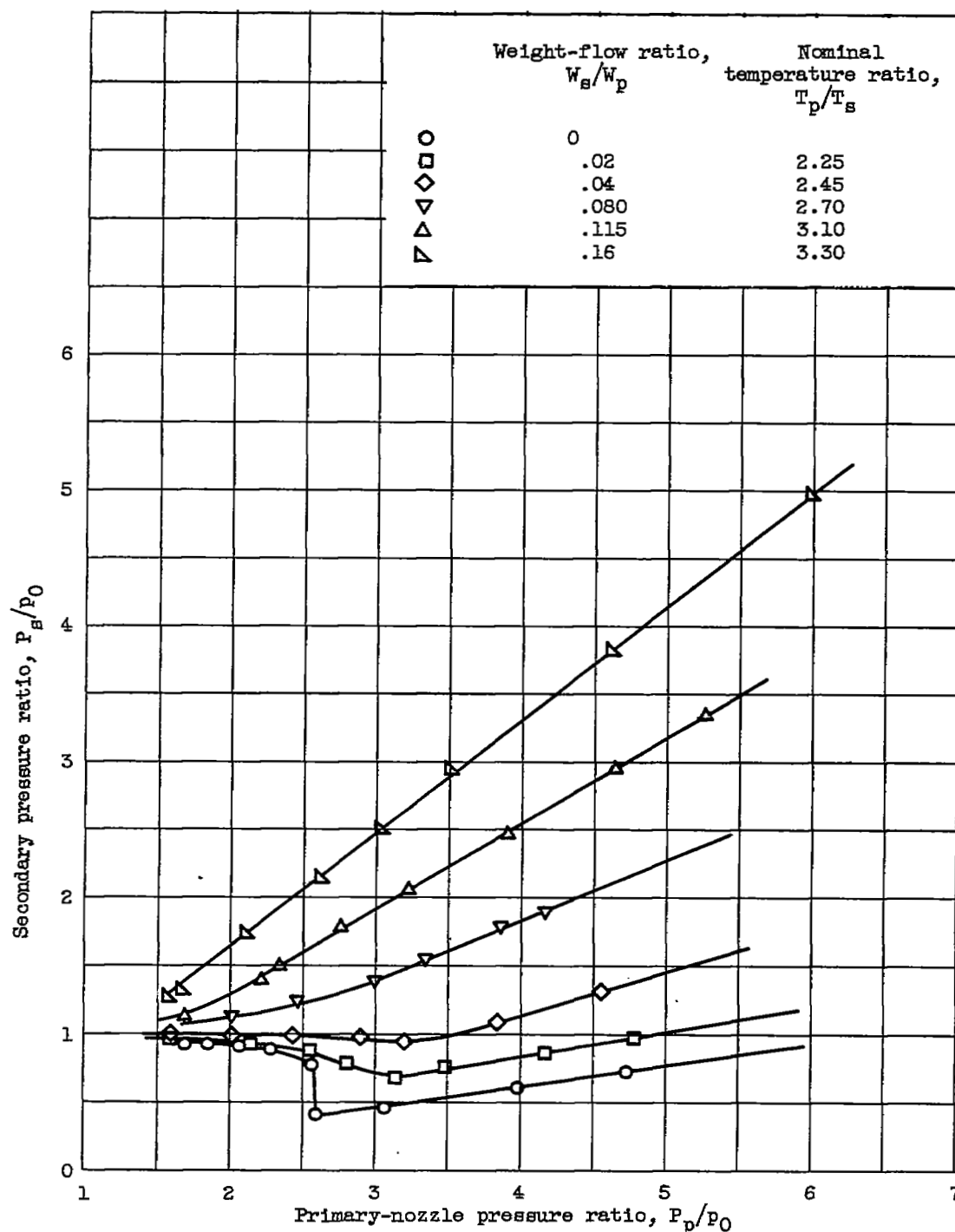
(g) Configuration 3; primary gas temperature, 3250° to 3400° R; diameter ratio, 1.31; spacing ratio, 0.4.

Figure 5. - Continued. Ejector pumping characteristics.



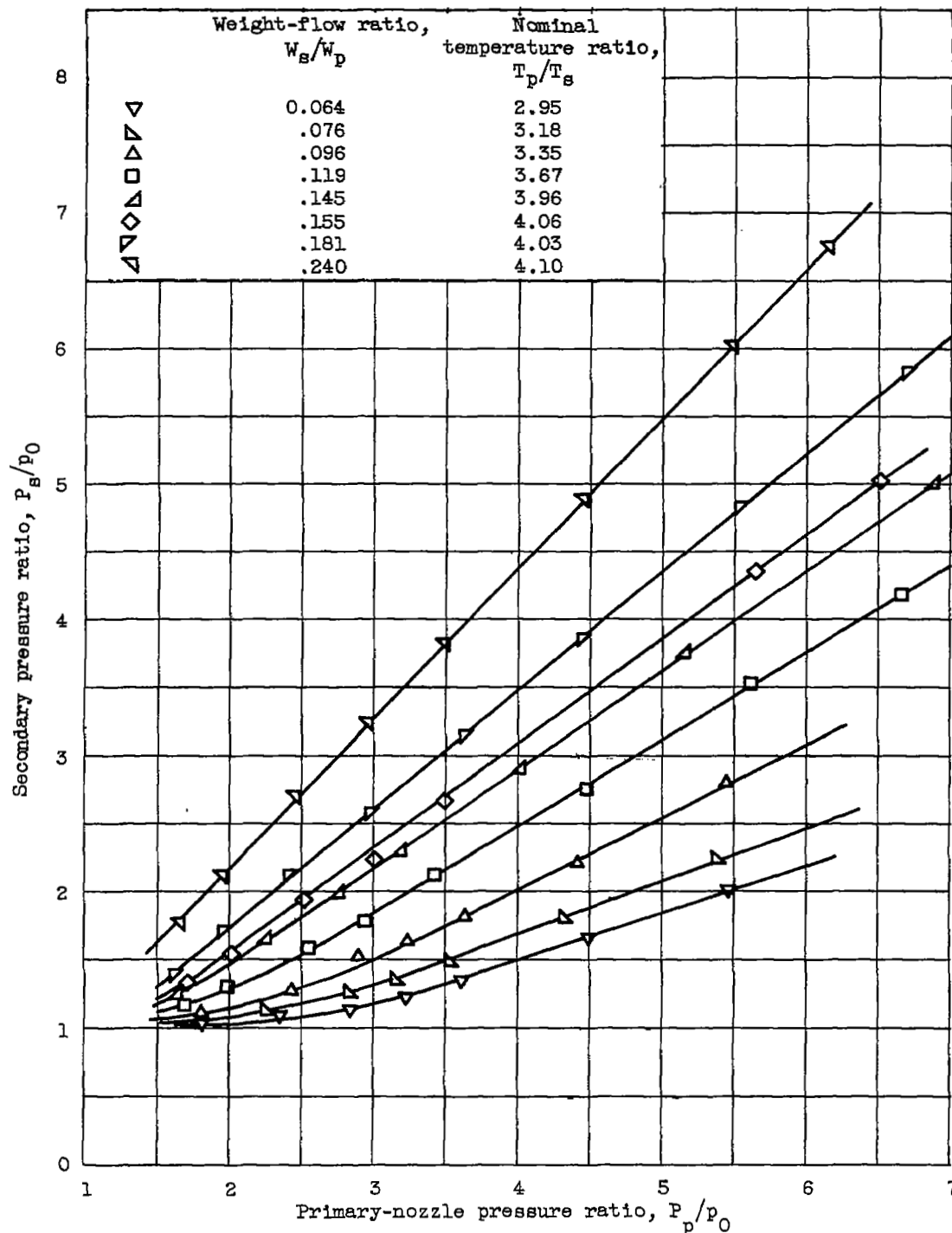
(h) Configuration 4; primary gas temperature, 1140° R; diameter ratio, 1.31; spacing ratio, 0.81.

Figure 5. - Continued. Ejector pumping characteristics.



(1) Configuration 4; primary gas temperature, 1900° to 2000° R; diameter ratio, 1.31; spacing ratio, 0.81.

Figure 5. - Continued. Ejector pumping characteristics.



(j) Configuration 4; primary gas temperature, 3200° to 3400° R; diameter ratio, 1.31; spacing ratio, 0.81.

Figure 5. - Concluded. Ejector pumping characteristics.

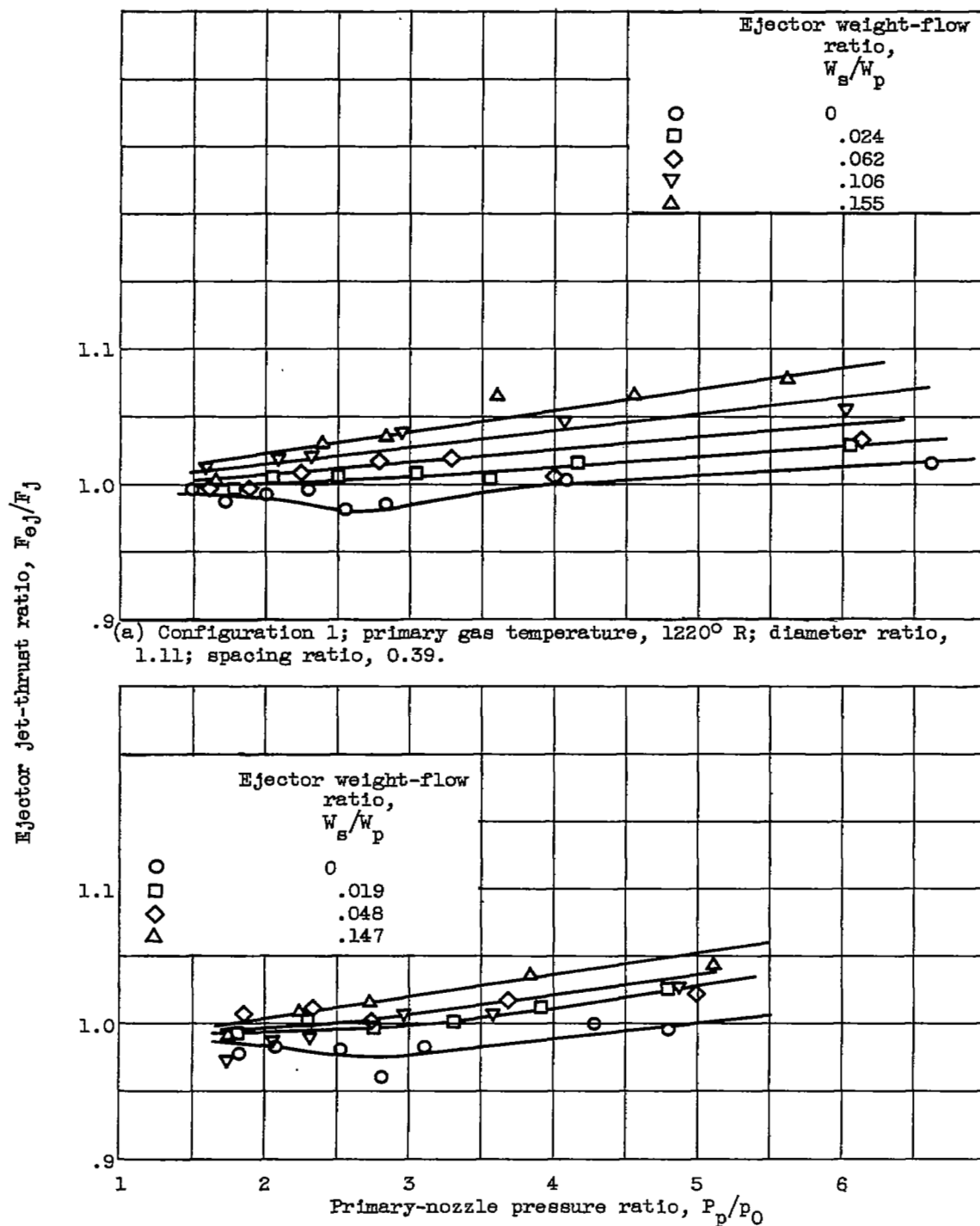
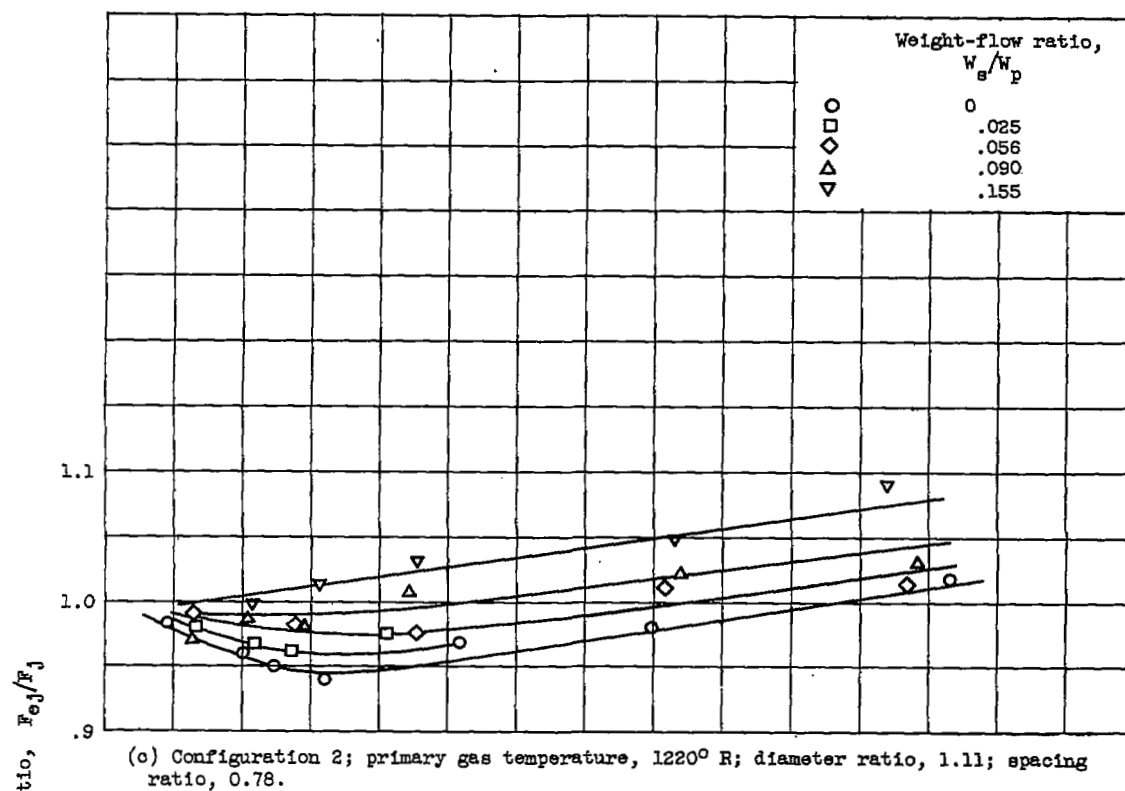
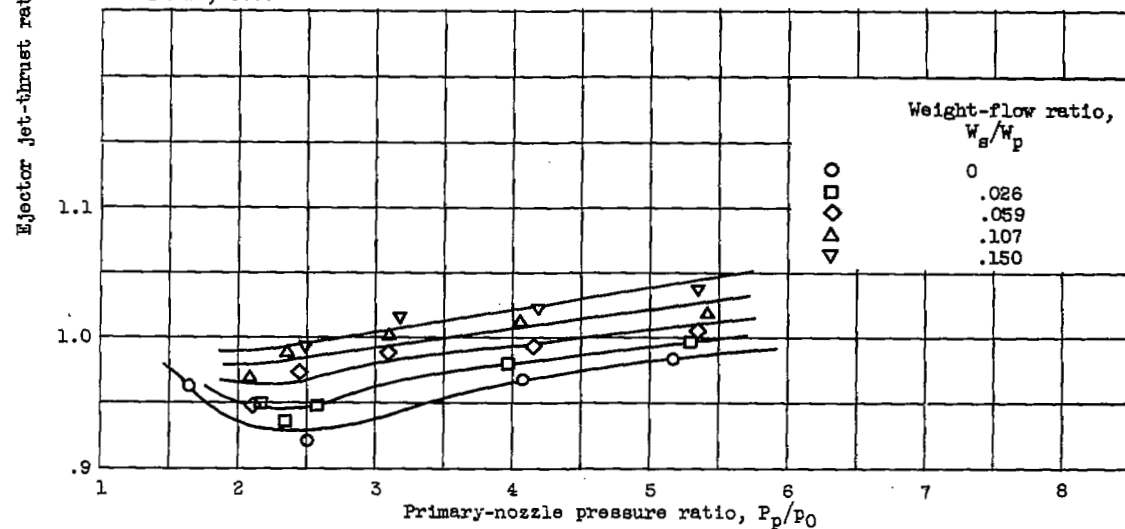


Figure 6. - Ejector thrust performance.

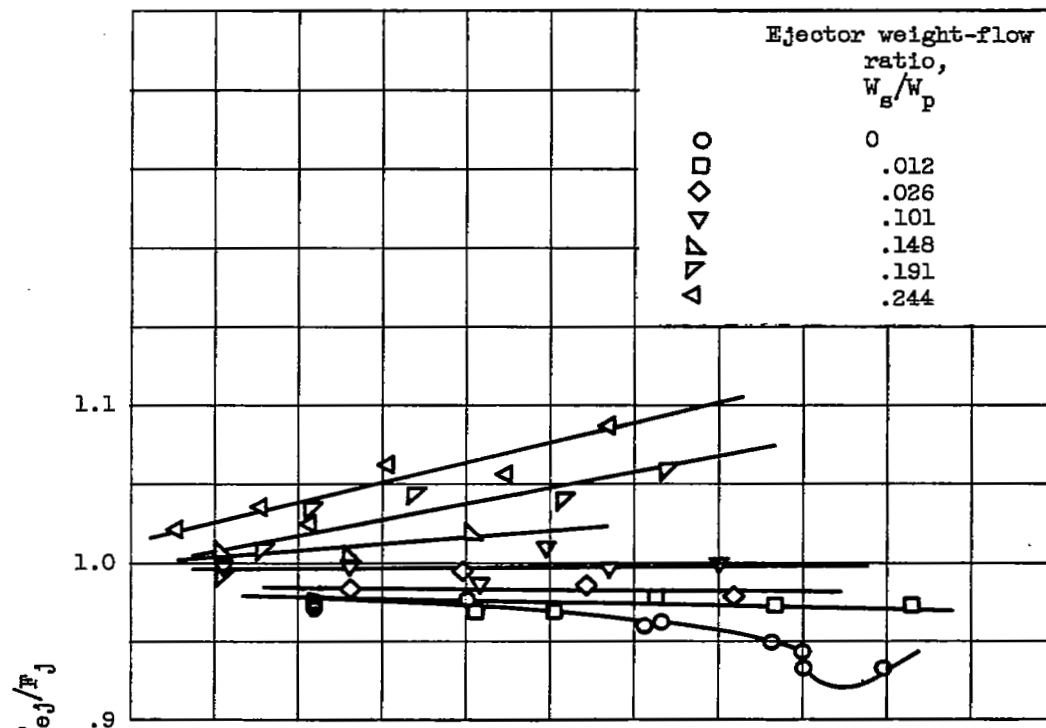


(c) Configuration 2; primary gas temperature, 1220° R; diameter ratio, 1.11; spacing ratio, 0.78.

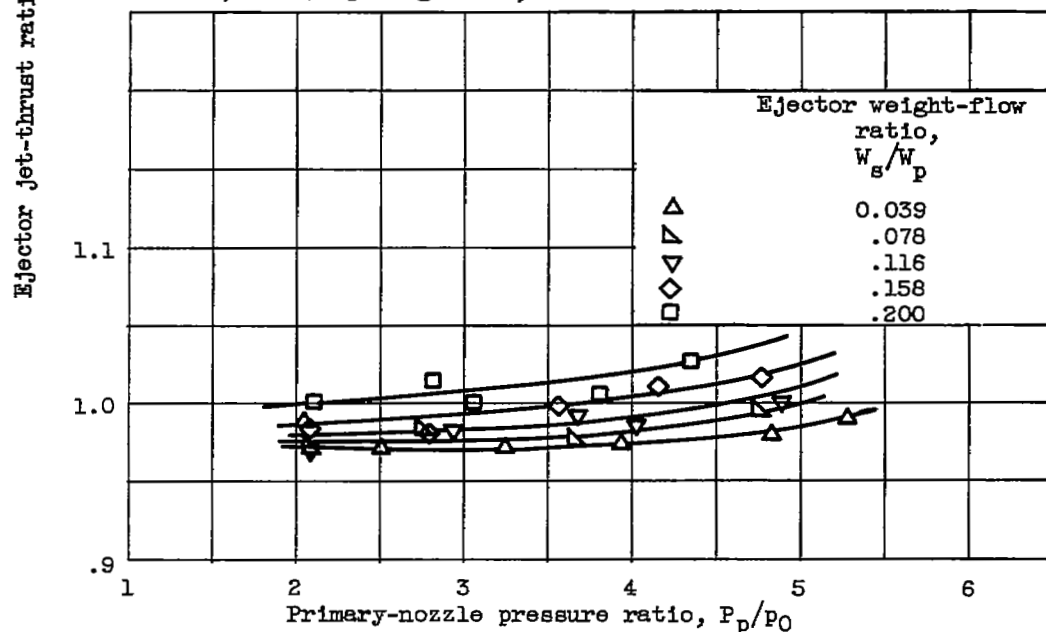


(d) Configuration 2; primary gas temperature, 1500° R; diameter ratio, 1.11; spacing ratio, 0.78.

Figure 6. - Continued. Ejector thrust performance.

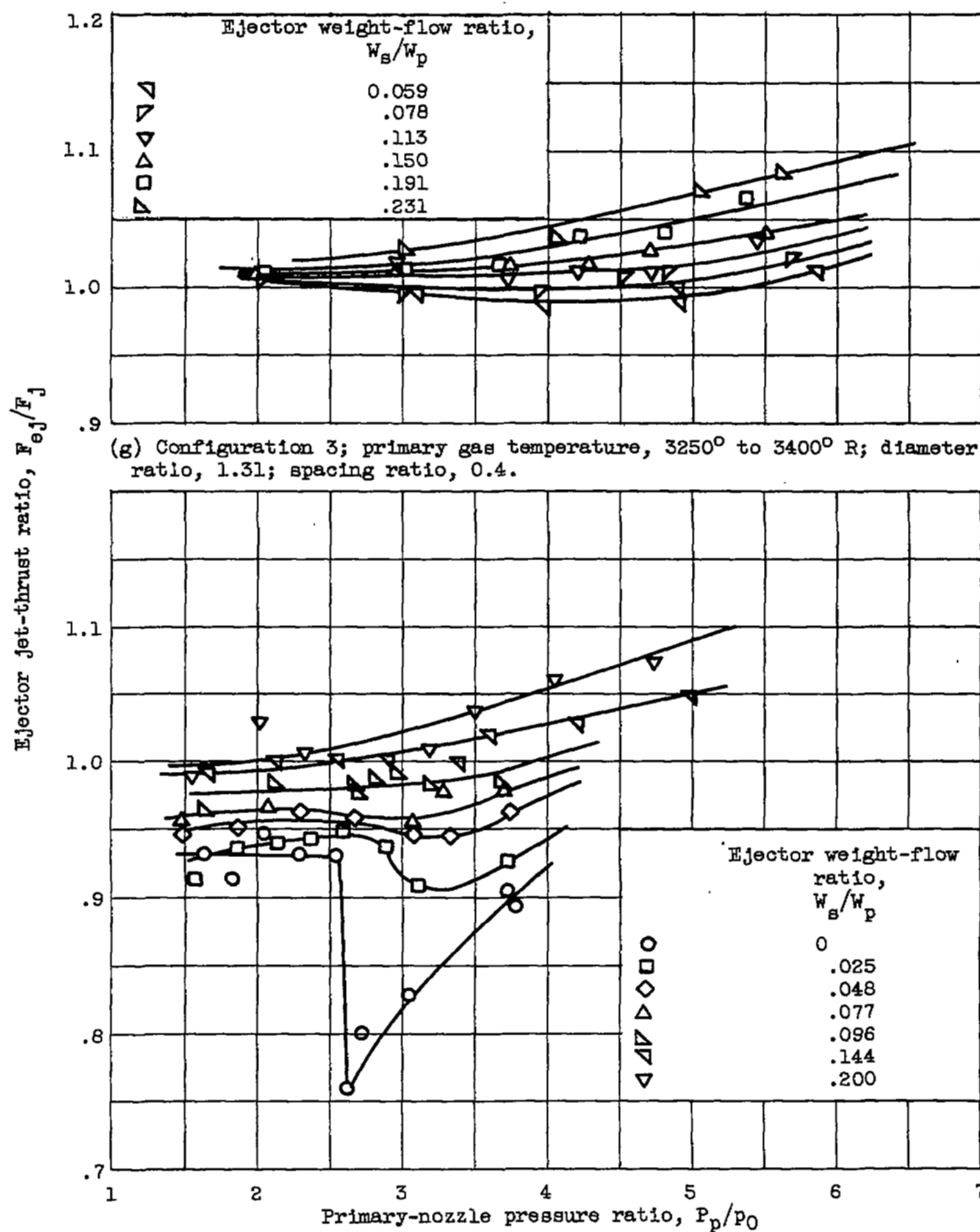


(e) Configuration 3; primary gas temperature, 1140° R; diameter ratio, 1.31; spacing ratio, 0.4.



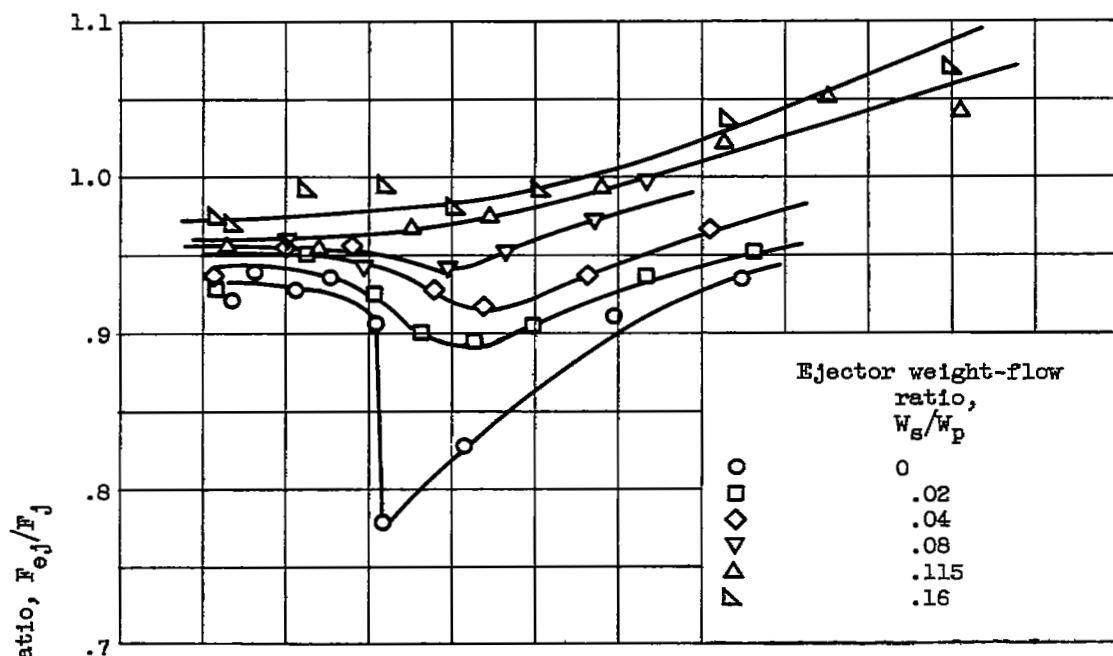
(f) Configuration 3; primary gas temperature, 2050° R; diameter ratio, 1.31; spacing ratio, 0.4.

Figure 6. - Continued. Ejector thrust performance.

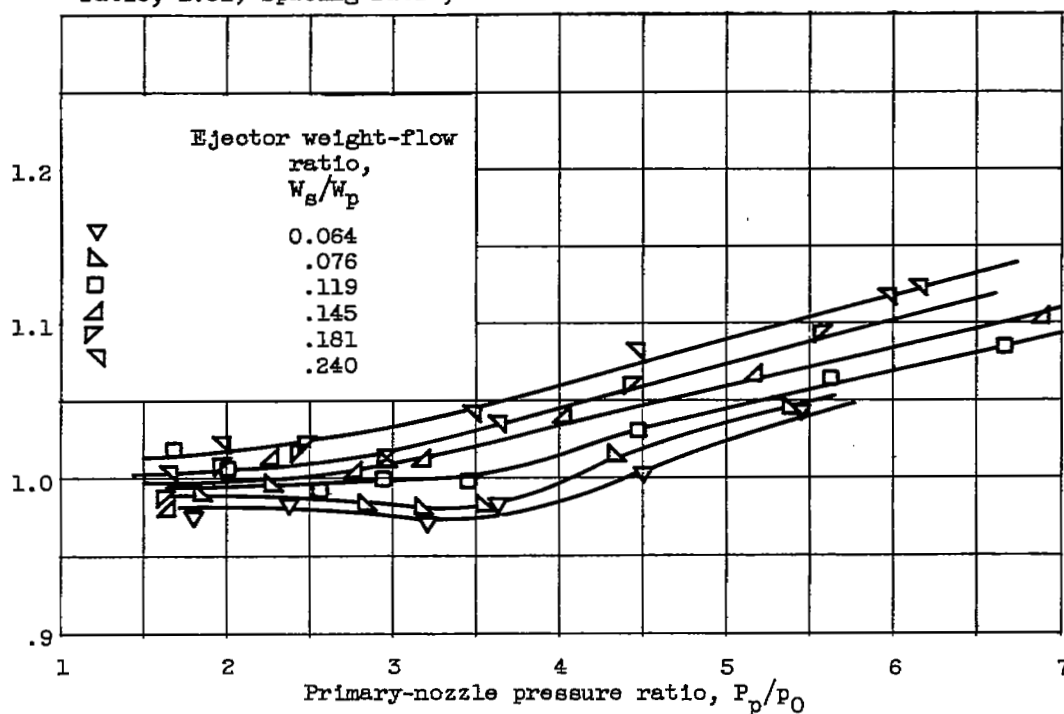


(h) Configuration 4; primary gas temperature, 1140° R; diameter ratio, 1.31; spacing ratio, 0.81.

Figure 6. - Continued. Ejector thrust performance.

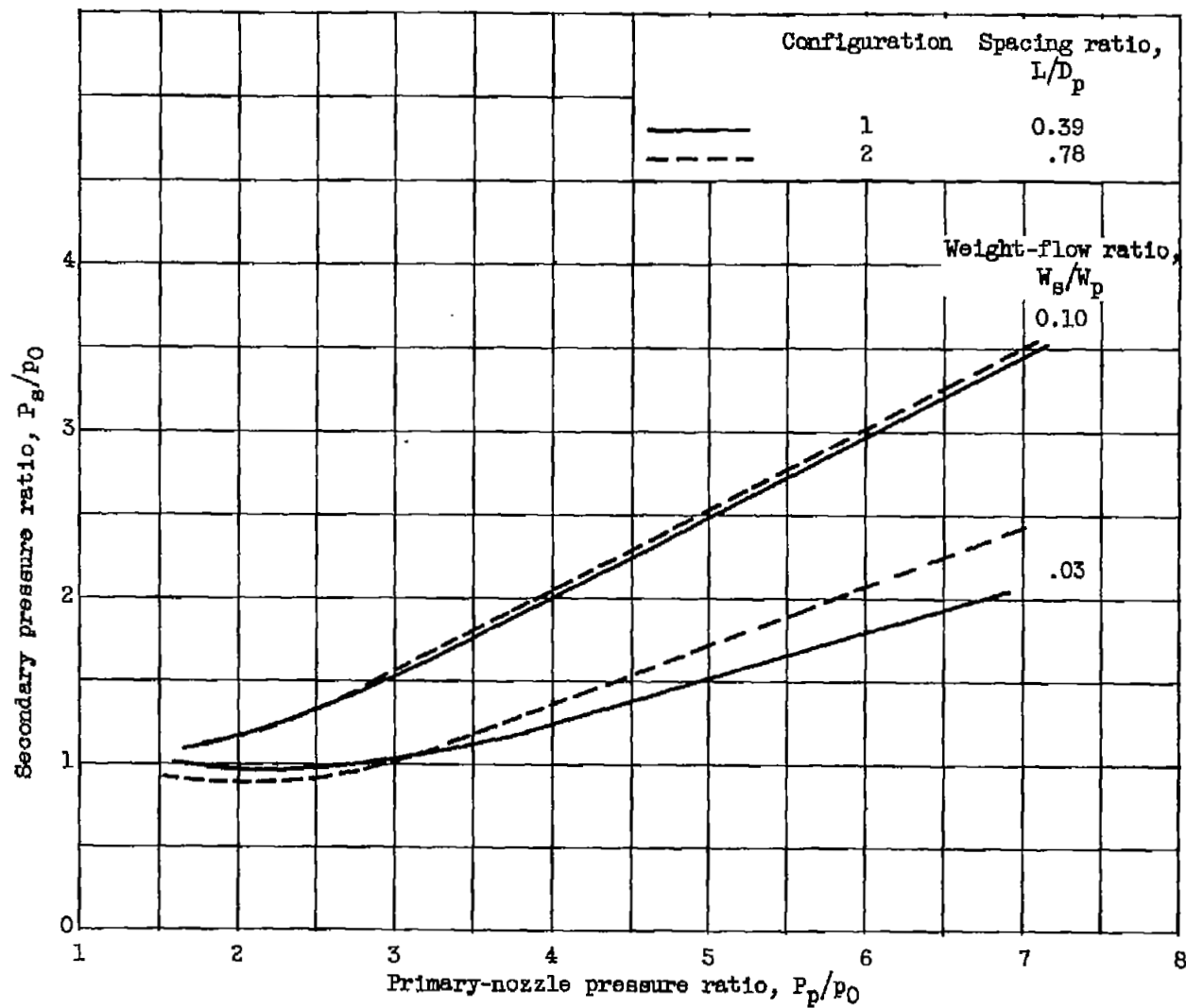


(i) Configuration 4; primary gas temperature, 1900° to 2000° R; diameter ratio, 1.31; spacing ratio, 0.81.



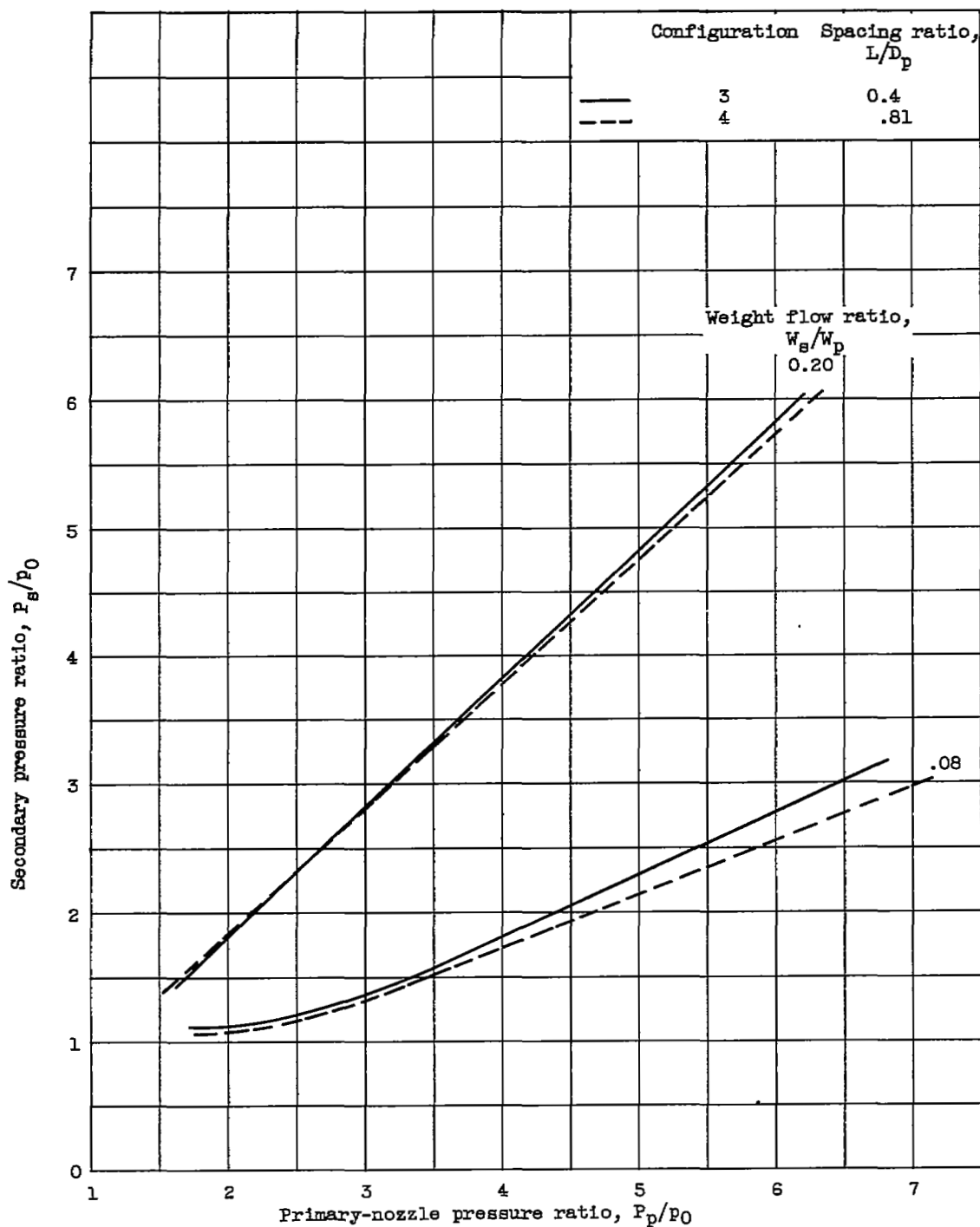
(j) Configuration 4; primary gas temperature, 3200° to 3400° R; diameter ratio, 1.31; spacing ratio, 0.81.

Figure 6. - Concluded. Ejector thrust performance.



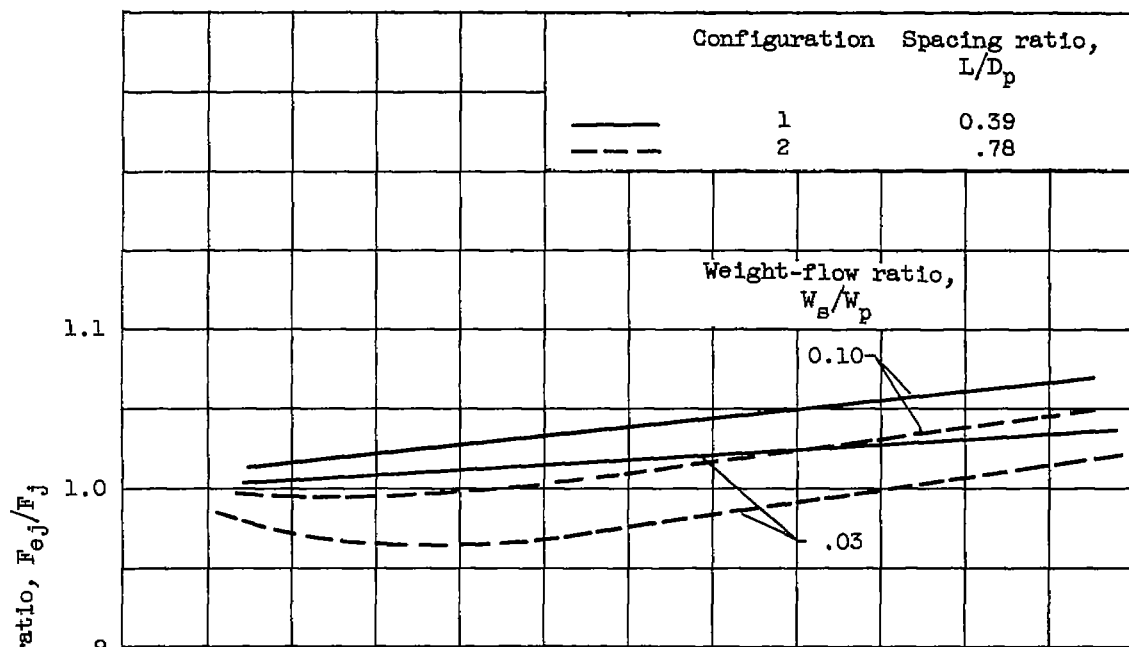
(a) Configurations 1 and 2; primary gas temperature, 1220° R; diameter ratio, 1.11.

Figure 7. - Effect of spacing ratio on ejector pumping characteristics.

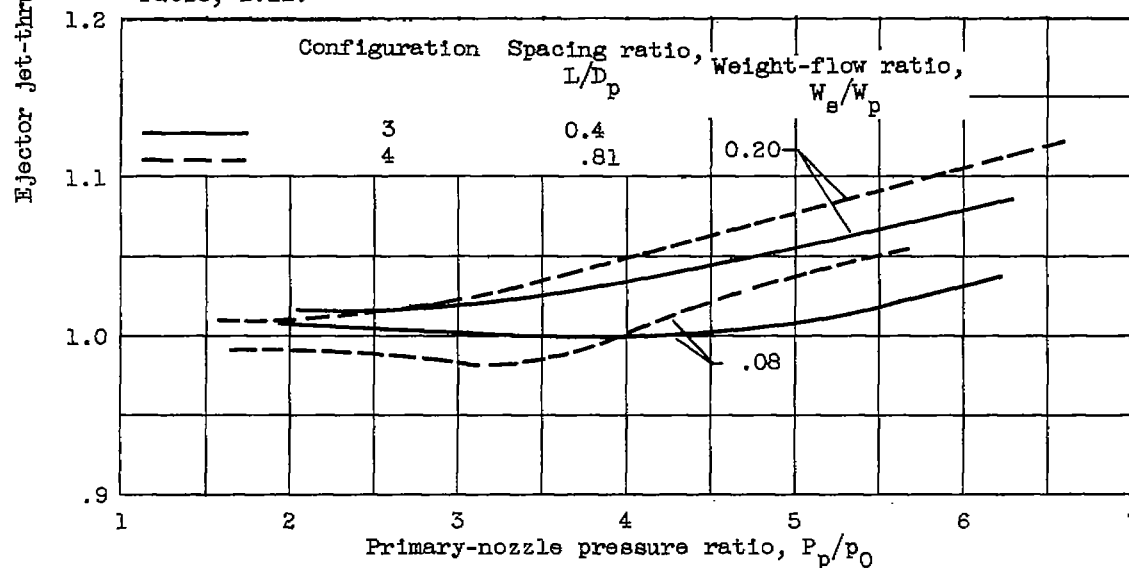


(b) Configurations 3 and 4; primary gas temperature, 3200° to 3400° R; diameter ratio, 1.31.

Figure 7. - Concluded. Effect of spacing ratio on ejector pumping characteristics.

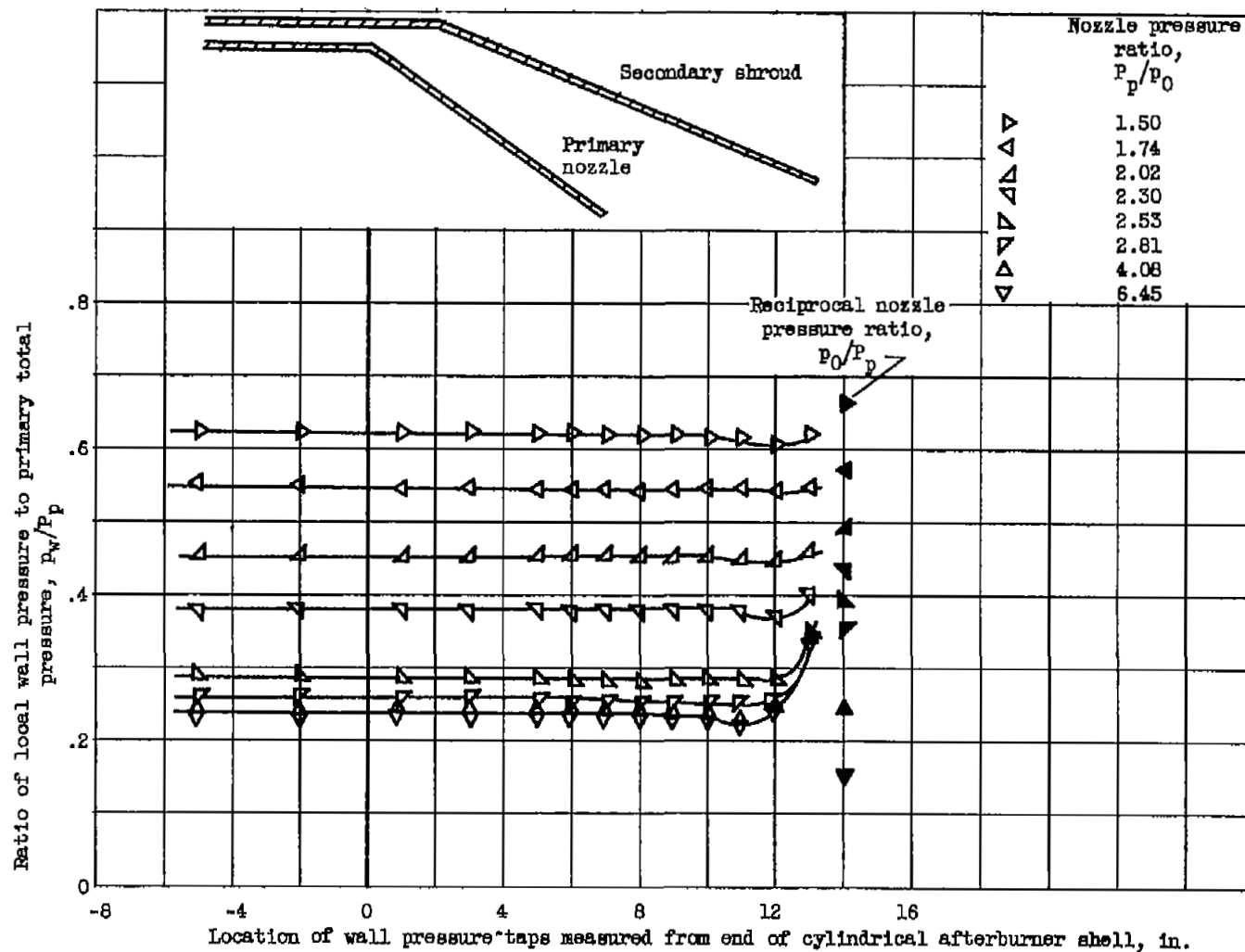


(a) Configurations 1 and 2; primary gas temperature, 1220° R; diameter ratio, 1.11.



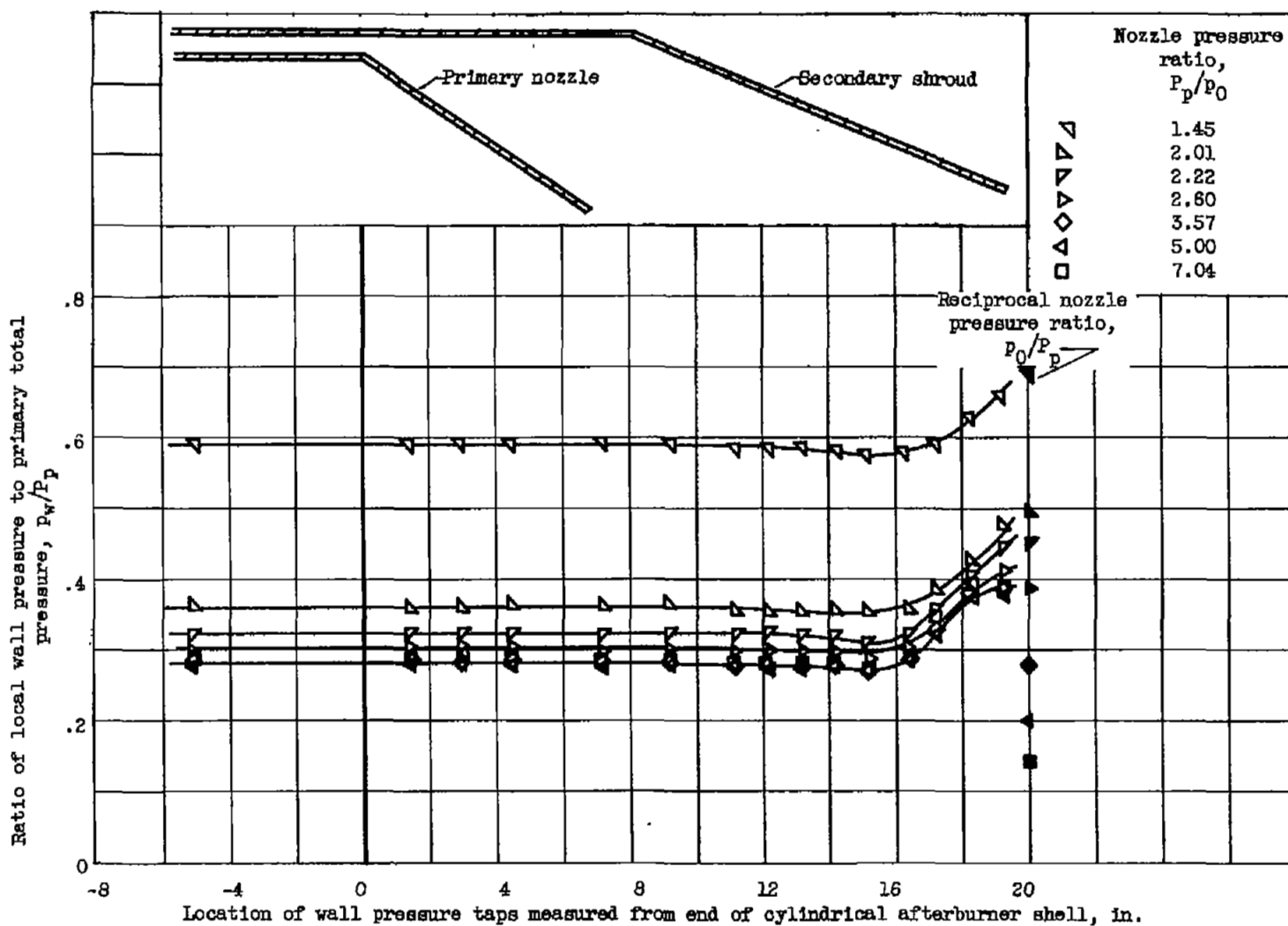
(b) Configurations 3 and 4; primary gas temperature, 3200° to 3400° R; diameter ratio, 1.31.

Figure 8. - Effect of spacing ratio on ejector thrust performance.



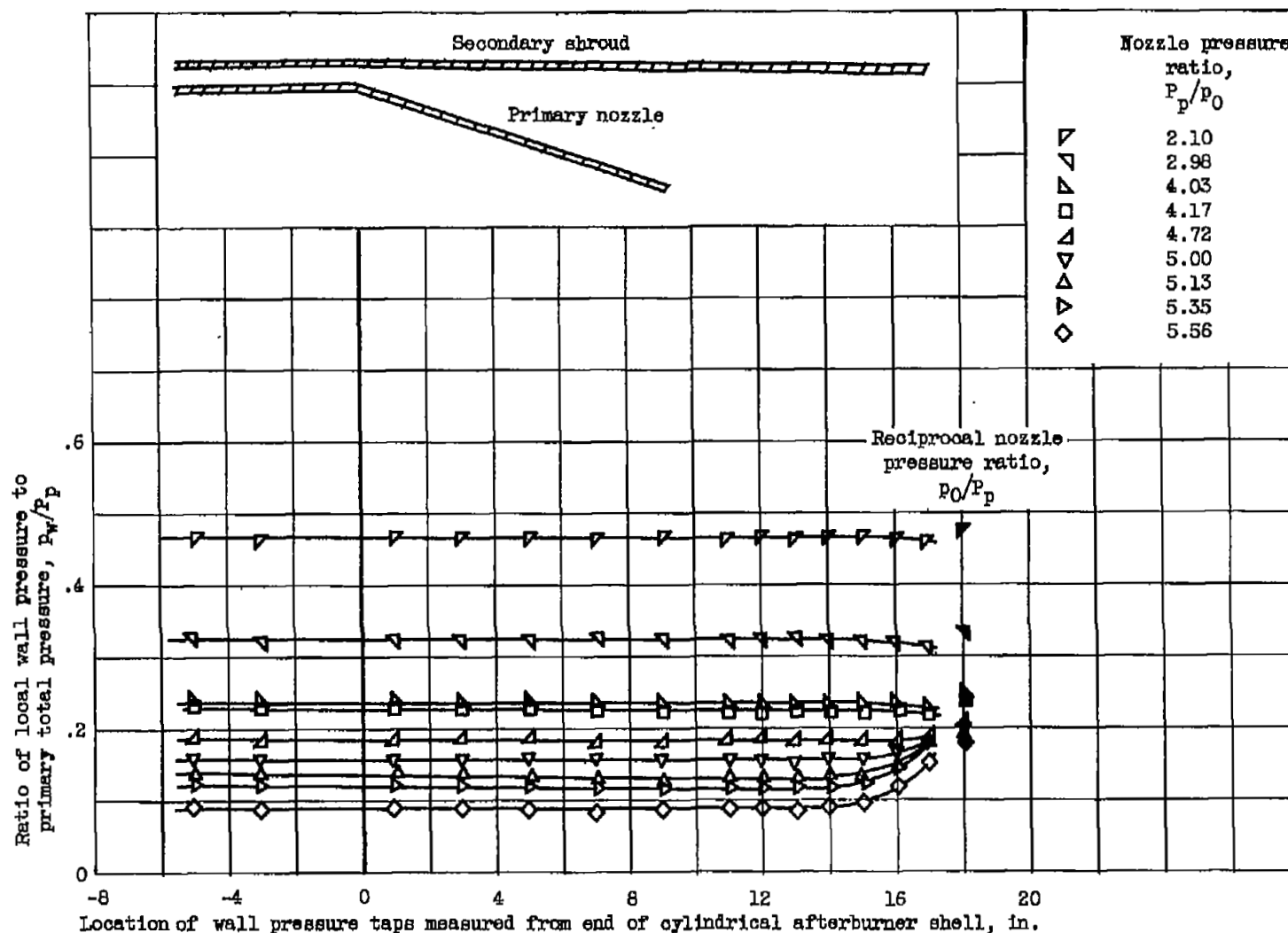
(a) Configuration 1; zero secondary weight flow; primary gas temperature, 1220° R; diameter ratio, 1.11; spacing ratio, 0.39.

Figure 9. - Ejector-shroud wall pressure distribution.



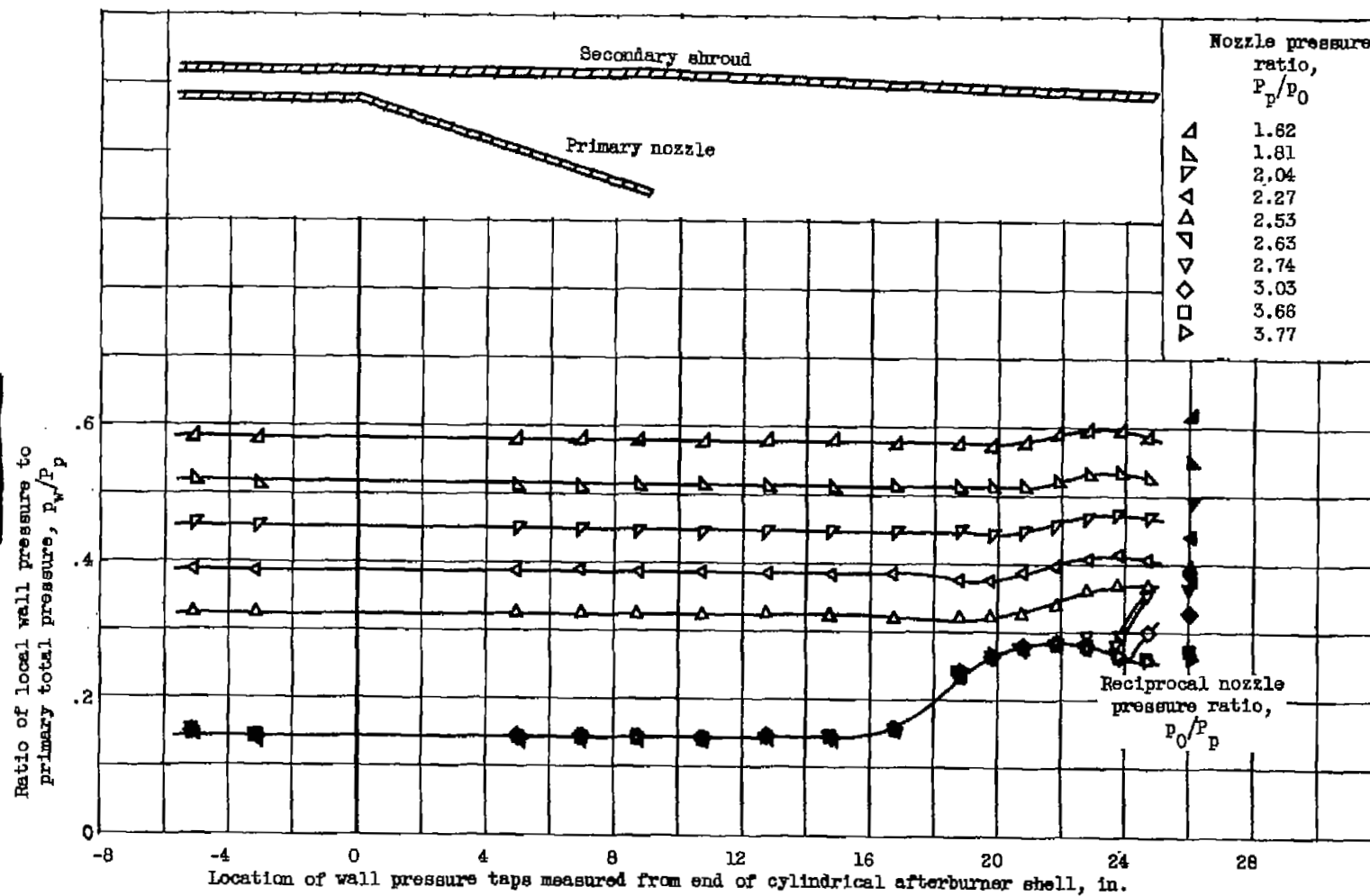
(b) Configuration 2; zero secondary weight flow; primary gas temperature, 1220° R; diameter ratio, 1.11; spacing ratio, 0.78.

Figure 9. - Continued. Ejector-shroud wall pressure distribution.



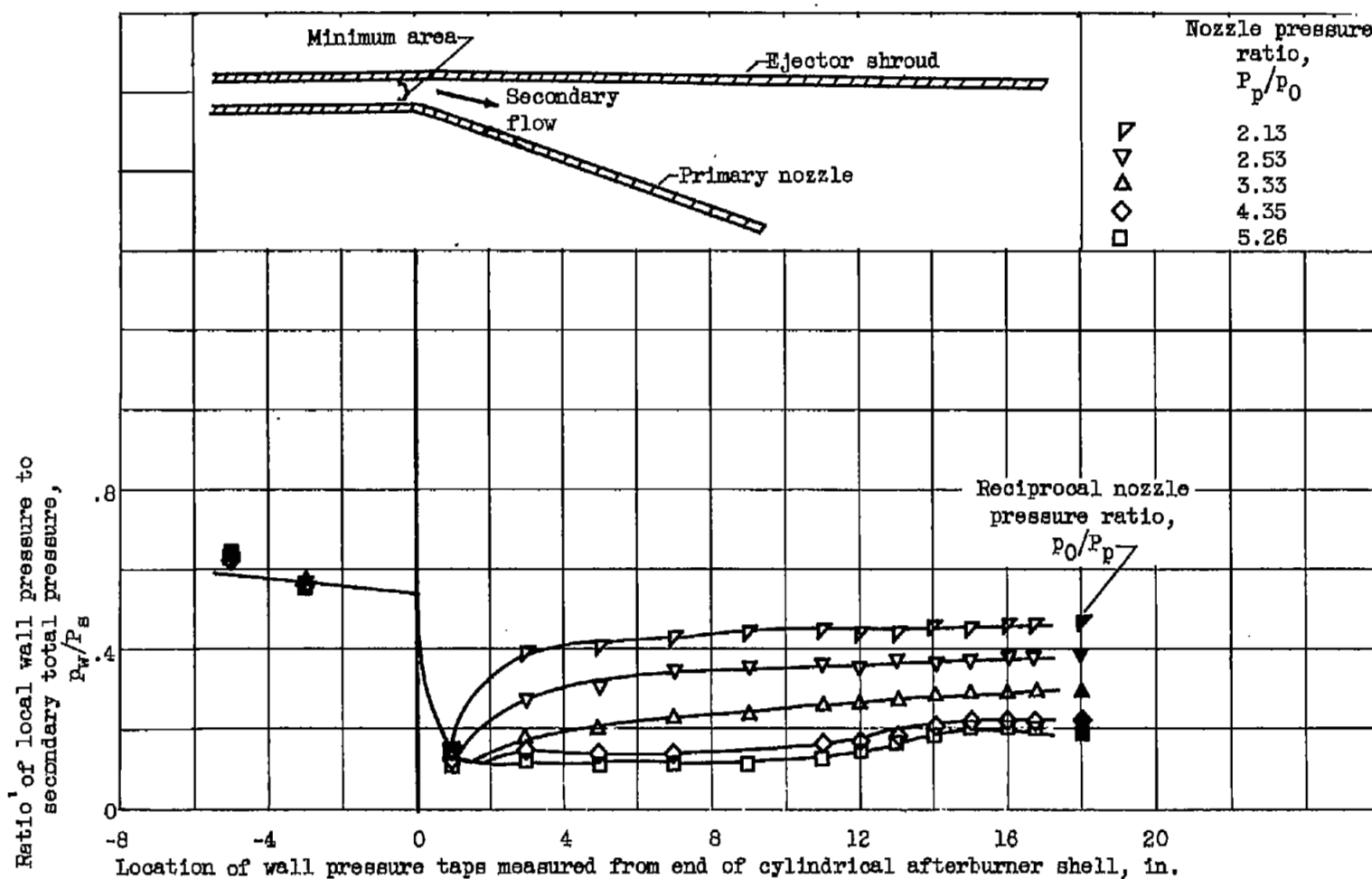
(c) Configuration 3; zero secondary weight flow; primary gas temperature, 1140° R; diameter ratio, 1.31; spacing ratio, 0.4.

Figure 9. - Continued. Ejector-shroud wall pressure distribution.



(d) Configuration 4; zero secondary weight flow; primary gas temperature, 1140° R; diameter ratio, 1.31; spacing ratio, 0.81.

Figure 9. - Continued. Ejector-shroud wall pressure distribution.



(e) Configuration 3; weight-flow ratio, 0.191; primary gas temperature, 1140° R.

Figure 9. - Concluded. Ejector-shroud wall pressure distribution.

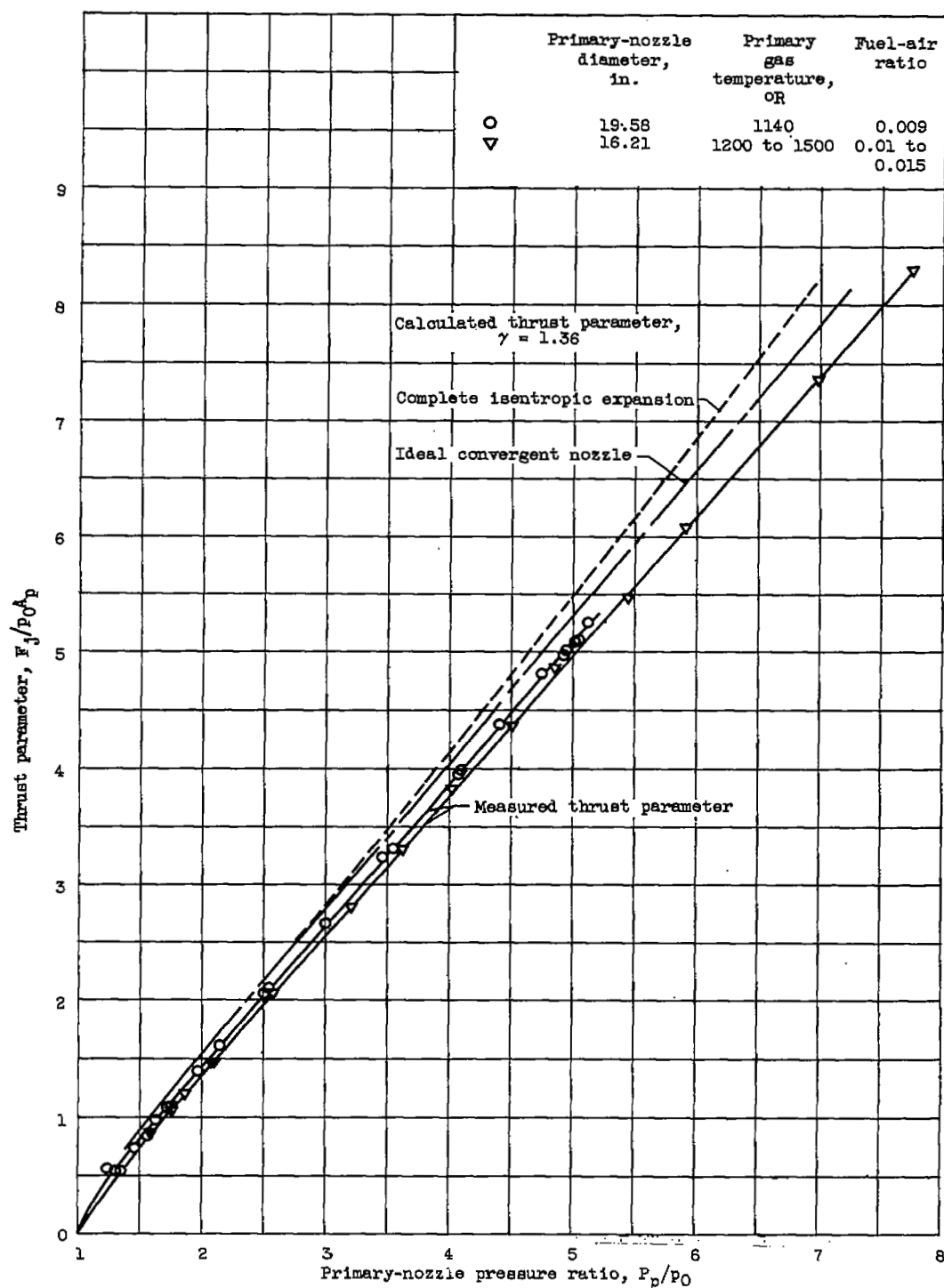
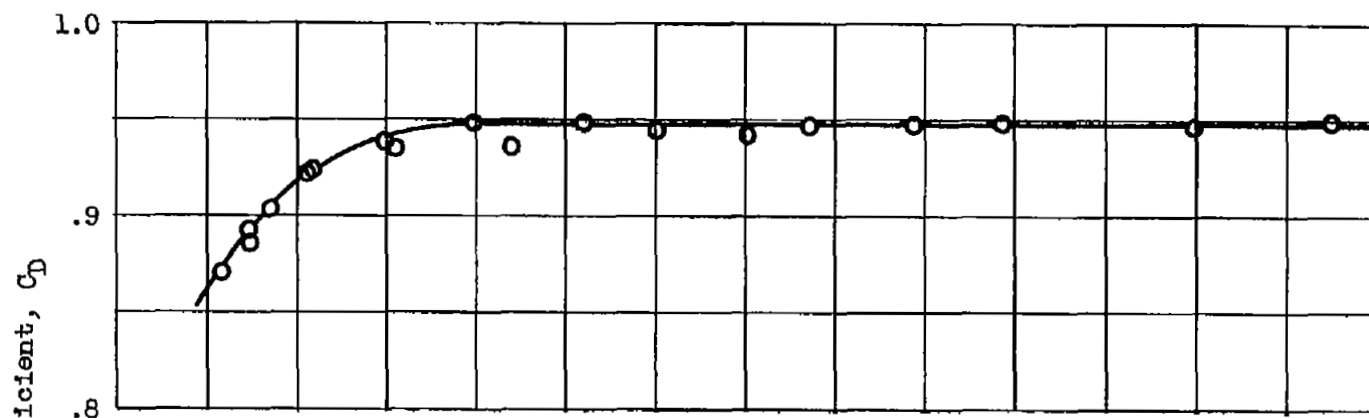
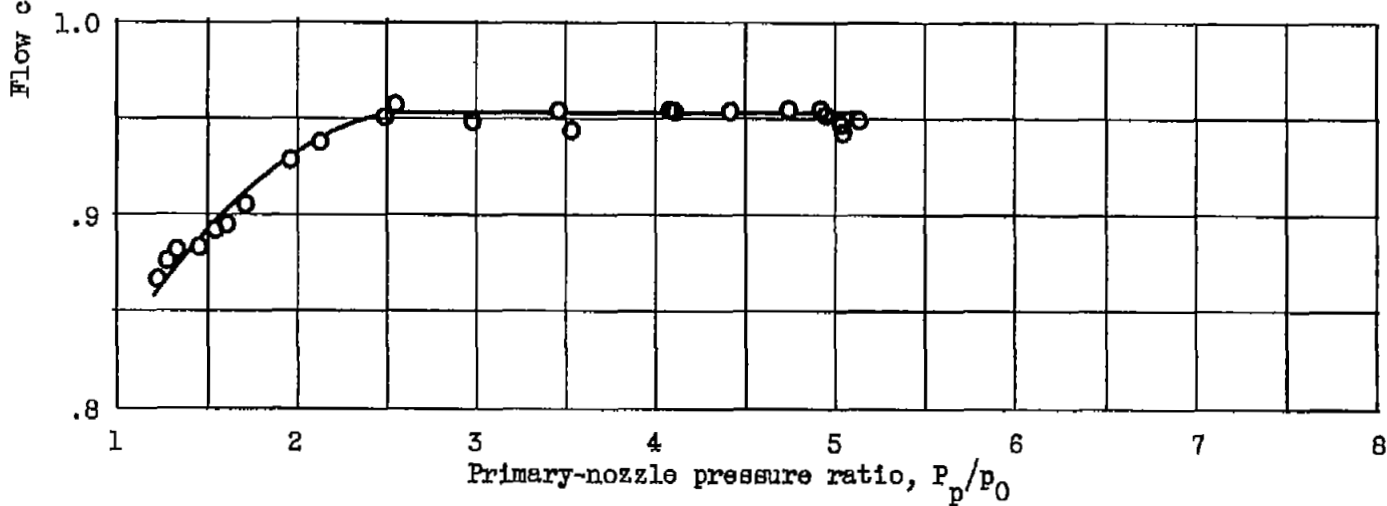


Figure 10. - Comparison of theoretical thrust parameters and measured thrust parameter of both 19.58-inch- and 16.21-inch-diameter primary nozzles without ejector shroud.



(a) 16.21-Inch-diameter primary nozzle; primary gas temperature, 1200° to 1500° R.



(b) 19.58-Inch-diameter primary nozzle; primary gas temperature, 1140° R.

Figure 11. - Flow coefficients of conical primary nozzles.

NASA Technical Library



3 1176 01435 4105

